

Carl von Ossietzky Universität Oldenburg

BACHELOR THESIS
IN ENGINEERING PHYSICS

REAL TIME ANALYSIS
OF FEL RADIATION SPECTRA
FOR THE ESTIMATION OF PHOTON PULSE DURATION

SUBMITTED BY

ROBIN ENGEL

*Carl-von-Ossietzky Universität Oldenburg
Deutsches Elektronen Synchrotron
Hochschule Emden/Leer*

SUPERVISORS

PROF. ULRICH TEUBNER
Hochschule Emden/Leer

GÜNTER BRENNER
Deutsches Elektronen Synchrotron

OLDENBURG, JANUARY 2015

CARL-VON-OSSIETZKY UNIVERSITÄT OLDENBURG
HOCHSCHULE EMDEN / LEER
DEUTSCHES ELEKTRONEN SYNCHROTRON

Abstract

Bachelor of Engineering

Real Time Analysis of FEL Radiation Spectra for the Estimation of Photon Pulse Duration

by Robin ENGEL

One of the most challenging tasks for extreme ultraviolet, soft and hard X-ray free-electron laser photon diagnostics is the precise determination of the photon pulse duration, which is typically in the sub 100 fs range. For some purposes like the FEL tuning, an estimate of the pulse duration is required in real time and with minimal experimental effort. Therefore a method has been developed to evaluate the photon pulse spectra during run-time, yielding an estimate for the photon pulse duration. The developed method makes use of the statistical properties and spectral correlation techniques and has been embedded into the Data Acquisition System of the FLASH facility.

Acknowledgements

First of all, I would like to thank my supervisors, Stefan Düsterer and Günter Brenner, whose great support I could always count on, and Ulrich Teubner, who made this project possible to begin with.

This project required me to combine knowledge from many areas of expertise, which I could not possibly have done without the help of many other colleagues here at DESY. One of them is Vladimir Rybnikov, who introduced me to and assisted me in the handling of DESY's data acquisition and control systems. Also in the IT area, Sören Grunewald introduced me to the UNIX-based DESY network, and Raimund Kammering helped me with the compilation and implementation of MATLAB-based programs into this network. Further thanks goes to Siarhei Dziarzhyski, who also helped me with the PG2 beamline and to Minjie Yan for making the LOLA measurements in this work possible. Many more helped me with advice on theoretical questions, background knowledge and organization, whom I can not name here. I would like to thank all those and also the rest of the FS-FL group, for making my time here so productive and enjoyable.

List of Figures

2.1	Schematic layout of FLASH [1]	3
2.2	Example of the development of microbunching along the undulator. The plots show the modulation of the electron density at the undulator entrance (left), within the exponential growth region (middle), and at the undulator exit (right) [2].	4
2.3	This undulator gain curve shows the energy in the radiation curve vs. undulator length. The error bars represent the uncertainty of $\pm 15\%$ in the calibration of the detector. [3]	5
2.4	FEL Photon pulse structure. (a) shows the structure in the time domain. The width of the temporal modes is characterized by the SASE coherence time T_{coh} . (b) shows the structure in the frequency domain. The width of the peaks is inversely proportional to the pulse duration T . (c) shows the structure in the frequency domain, averaged over several shots. The width of the spectrum is inversely proportional to the temporal coherence T_{coh} [4].	8
2.5	Evolution of the PEPDD from end of the linear regime down to deep saturation regime, measured in covered undulator distance z . Left and right columns correspond to an overall electron bunch charge of 0.5 and 1 nC, respectively. Solid lines show the gamma distribution. The standard deviation of the PEPDD is given as σ . [5]	9
3.1	a) A summation over 395 FLASH radiation spectra. The green area is within the FWHM boundaries. b) The second order correlation function computed from the spectra with two theoretical fits. The fit parameters σ_T and T represent the rms bandwidth of a Gaussian pulse and the duration of a flat-top pulse respectively. Because the stability of the measured second order correlation function decreases with correlation distance, the fit only regards small correlation distances, underlaid with light green.	12
4.1	Schematic layout of the PG2 monochromator beamline at FLASH. The mirrors M0 to M4 are indicated in green, the plane grating G in red. The exit slit S can be replaced by a Ce:YAG screen for spectrometer mode. [6]	20
4.2	Schematic view of the MGU, consisting of the grating G and the premirror M2. Indicated are the angles of incident α and diffraction β	21
4.3	A plot of the unaltered camera image from the end of the PG monochromator beamline. We observe a tilt of the spectral lines.	22
4.4	Working principle of the transverse deflecting structure LOLA. The longitudinal electron bunch profile is streaked by a RF wave and thereby converted into a transverse structure that is detectable on a projection screen. [7]	23

4.5	A simplified schematic of the TDS LOLA at FLASH. Quadrupole magnets are neglected for simplicity. [8]	24
5.1	Dispersed LOLA measurement taken at 05.09.2015, 15:49. In the particular measurement shown in this Figure, the electron bunch exhibits two maxima in the phase space, which is a result of non-optimal FEL tuning. As our theoretical model does not cover the case of multiple maxima, the weaker maximum has been neglected and the Gaussian fit to the higher maximum has been used for the measurement. The estimated relative SASE gain bandwidth with electron chirp amounts to 0.452% FWHM.	27
5.2	Control panel of the Photon Pulse Length server. The plots on the left show the input spectra (up to down) directly from the camera, after the low-pass filtering and the accumulated spectrum over the last 300 spectra. The plot to the upper right shows the calculated second order correlation function including the fits for Gaussian and flat-top electron bunches. The measurement result for the Gaussian electron bunch shape, averaged over the last 50 calculations and corrected for electron bunch chirp is displayed to the lower right, including the standard deviation. Measurement taken at 05.09.2014, 17:30.	29
5.3	Picture of the Statistic Spectra Analysis GUI.	31
5.4	An overview plot of 4053 Spectra. The red line represents the average spectrum. The Measurement taken at 05.09.2014, 18:49.	32
5.5	Plot generated with the Count Maxima button. The plots show (up to down) the average spectrum of all considered spectra, a selected example spectrum before filtering, the same example spectrum after filtering and the number of spectral spikes within the whole spectrum over the event index. Measurement taken at 05.09.2014, 18:49.	34
5.6	First plot generated with the Analyze Intesity Distribution button. The left column shows the development of pulse energy within the FWHM window (a) and the line windows (c) and (e) around the two selected frequencies. The right column shows the measured and calculated PEPDD for the same spectral windows. Measurement taken at 05.09.2014, 18:49.	35
5.7	Second plot generated with the Analyze Intesity Distribution button. Plot (a) illustrates the selected windows in the averaged spectrum, plot (b) shows the M-values of frequency windows around the selected wavelength with a variable window width. Plot (c) shows the M-Values of the line windows marked in (a) at their respective relative frequency and (d) shows the averaged curve of the ones displayed in (b). Measurement taken at 05.09.2014, 18:49.	36
5.8	Result plot of a multiple correlation run. Each bar represents one measurement. The red line is the averaged pulse durations. In this case, each measurement used a set of 150 spectra with an increment of 50 spectra. The Plot also shows the DAQ event ID and exact time of the first spectrum.	39

6.1	The graphs show the temporal development of the measured pulse duration in comparison to the relative shot energy. The blue bars each represent single measurements, the red line the averaged pulse duration measured with second order correlation method, the blue line is measured with the spike counting method. The green line shows the averaged shot energy, normalized to fit the scale. Measurement taken 05.09.2014, upper plot 20:45 to 20:50, total of 2995 spectra; lower plot 18:49 to 18:56, total of 4053 spectra, each second order correlation calculation considered a package of 150 spectra.	41
6.2	Measurement with different apertures. The vertical apertures correspond to the dispersive direction of the spectrometer. Measurements taken 05.09.2014 between 19:44 and 20:50.	43
6.3	Second order correlation and spike counting measurements compared to measurements of the electron bunch duration with varied electron bunch charges. Measurements taken 05.09.2014 between 22:07 and 22:29.	45

List of Tables

4.1	Parameters of the optical elements of the beamline according to Figure 4.1. Table from [9].	20
6.1	Comparison of electron bunch duration measurements using the LOLA TDS (rms) and the photon pulse duration measured by the multiple correlation method (single line spectra) and the spike counting method at different electron bunch charges. Taken 05.09.2014.	46

Abbreviations

DAQ	<u>D</u> ata <u>A</u> c <u>Q</u> uision system
DOOCS	<u>D</u> istributed <u>O</u> bject <u>O</u> riented <u>C</u> ontrol <u>S</u> ystem
FEL	<u>F</u> ree- <u>E</u> lectron <u>L</u> aser
FLASH	<u>F</u> ree-electron <u>L</u> ASer in <u>H</u> amburg
FWHM	<u>F</u> ull <u>W</u> idth <u>H</u> alf <u>M</u> aximum
ICCD	<u>I</u> ntensified <u>C</u> harge <u>C</u> oupled <u>D</u> evice
HHG	<u>H</u> igh <u>H</u> armonic <u>G</u> eneration
LINAC	<u>L</u> INear <u>A</u> Ccelerator
MGU	<u>M</u> irror <u>G</u> rating <u>U</u> nit
PEBDD	<u>P</u> ulse <u>E</u> nergy <u>P</u> robability <u>D</u> ensity <u>D</u> istribution
PG	<u>P</u> lane <u>G</u> rating
RF	<u>R</u> adio <u>F</u> requency
SASE	<u>S</u> elf <u>A</u> mplified <u>S</u> pontaneous <u>E</u> mission
TDS	<u>T</u> ransverse <u>D</u> eflecting <u>S</u> tructure
WAU	<u>W</u> ater-cooled <u>A</u> perture <u>U</u> nit
XUV	<u>E</u> xtr <u>U</u> ltra <u>V</u> iolet

Physical Constants

Speed of Light	c	$=$	$2.997\,924\,58 \times 10^8 \text{ ms}^{-1}$
Electron Charge	e	$=$	$-1.602\,176\,56 \times 10^{-19} \text{ As}$
Electron Mass	m_e	$=$	$9.109\,382\,91 \times 10^{-31} \text{ Kg}$

Symbols

c_{ff}	Fixed focus constant of the monochromator	-
g_1	First order spectral correlation function	-
g_2	Second order spectral correlation function	-
n_ω	Number of spikes per unit frequency	-
t	Time	s
t_k	Random electron arrival time at undulator entrance	s
E	Electric field	V/m
E_{kin}	Kinetic energy	J
$F(t)$	Electron bunch form function	-
I_e	Electric current	A
K	Undulator parameter	kg s cm
L_{sat}	FEL saturation length	m
M	Number of modes	-

N	Number electrons contributing to the SASE process	-
N_s	Number of maxima in the temporal photon pulse structure	-
N_ω	Number of spikes in a spectrum	-
S	Spectrometer signal	Counts
T	Pulse duration, Flat-Top Profile	s
T_{coh}	SASE coherence time, FWHM	s
T_{corr}	Photon pulse duration, corrected for electron chirp	s
W	Photon pulse radiation energy	J
γ	Relativistic factor	-
λ_u	Undulator period	m
λ_r	Fundamental undulator radiation wavelength	m
ρ	FEL parameter	-
σ_m	Spectrometer resolution rms width	rad/s
σ_T	Pulse duration, rms.	s
σ_{min}^{ph}	Minimal rms photon pulse duration.	s
σ_ω	SASE gain bandwidth, rms.	rad/s
σ'_ω	Photon pulse bandwidth in frequency domain, rms.	rad/s
τ_c	SASE coherence time, rms	s
ω	Angular frequency	rad/s
ω_0	Angular frequency of central wavelength	rad/s
$\Delta\omega$	Angular frequency width of spectral correlation window	rad/s
Γ	Gamma function	-
Ω_c	Spectral coherence of an ideal spectrum ¹	rad/s
Ω'_c	Spectral coherence of a real spectrum ²	rad/s

¹Generated by an unchirped electron bunch.

²Generated by a chirped electron bunch.

Contents

Abstract	ii
Acknowledgements	iii
List of Figures	iv
List of Tables	vii
Abbreviations	viii
Physical Constants	ix
Symbols	ix
Contents	xi
1 Introduction	1
2 FLASH	3
2.1 SASE - Self Amplified Spontaneous Emission	3
2.1.1 The Electron Bunch Shape	5
2.1.2 The two Regimes of Operation	6
2.2 Temporal and Spectral Photon Pulse Structure	7
2.3 Pulse Energy Statistics	7
3 Derivation of the Photon Pulse Duration	10
3.1 Spike Counting	10
3.2 Intensity Distribution	11
3.3 Second Order Correlation	12
3.3.1 Measured Correlation Function	13
3.3.2 Expected Correlation Function	14
3.4 Energy Chirp within the Electron Bunch	17
4 The Measurement Setup	19
4.1 The PG Monochromator Beamline	19
4.1.1 Tilt of Spectral Lines on the Spectrometer Screen	22
4.2 Transverse Deflecting Structure LOLA	23
5 Developed Evaluation Software	25
5.1 Developed Applications	25

5.2	Example Measurement	27
5.2.1	Dispersed TDS Measurement	27
5.2.2	PPL-Server Measurement	29
5.2.3	Extracting Spectra from the DAQ	30
5.2.4	Starting the SSA MATLAB GUI	31
5.2.5	Spectra Overview	32
5.2.6	Setting Filters	33
5.2.7	Spike Counting	34
5.2.8	Intensity Distribution	35
5.2.9	Single Second Order Correlation Run	37
5.2.10	Multiple Second Order Correlation Run	38
6	Measurements	40
6.1	Comparison and Temporal Stability	41
6.2	Apertures in the Photon Beam	43
6.3	Electron Bunch Charge	45
7	Conclusion and Outlook	47
A	MATLAB: Spectra Evaluation	49
B	MATLAB: Data Handling	55
C	Diffraction from WAU	58
	Bibliography	59
	Conferences	61
	Declaration of Authorship	62

Chapter 1

Introduction

Since the discovery of synchrotron radiation sources in the 1960th, they have taken an important role in several fields of research. The first synchrotrons were built for the purpose of high energy physics to study collision processes of accelerated particles and synchrotron radiation was used parasitically as a side-product. The storage rings containing accelerated electrons provided radiation with low emittance and high brightness in a widely variable energy range. The electrons were usually accelerated in bunches, creating radiation pulses with a duration in the order of some 100 picoseconds. However, the spectral brilliance¹ was still comparatively low, as the wavelength of the radiated light scales inversely with the kinetic energy, and the radiative power scales with the number of accelerated particles.

Therefore the demand for storage rings dedicated solely to the generation of synchrotron radiation came up and led to the development of synchrotron radiation sources with increasing parameters like peak brightness, wavelength range and brilliance. Nowadays, synchrotron radiation facilities are long established as a standard tool not only in material sciences. However, the parameters of the synchrotron radiation were not comparable with the radiation of optical lasers in terms of coherence and peak brightness. High Harmonic Generation (HHG) is a method to transfer the intensity of a wave with a low photon energy to a wave with a multiple of the original photon energy using non-linear processes within an optical medium. In certain limits, the brilliance of optical lasers can be transferred to the XUV regime, but the conversion efficiency of HHG light sources

¹The spectral brilliance is the number of photons emitted per unit wavelength interval, time interval, solid angle and area.

decreases as going to short wavelengths.

Since the start of the 21st century, a fourth generation of synchrotron radiation sources revolutionized the field in form of the Free-Electron Laser (FEL), operating in the XUV and X-ray regimes. As the name suggests, FELs combine the high peak brilliance and transverse coherence of laser light sources with the freely variable wavelength range of synchrotron radiation facilities. In an FEL, the amplification medium in the resonator used by optical lasers is "replaced" with accelerated electrons passing through the spatially periodic magnetic field of an undulator. The thereby created radiation wavelength is a function of the undulator parameters and the kinetic energy of the electrons and is thus freely selectable. Compressing the electron bunch to very short pulses allows the generation of very intense pulses with durations in the femtosecond timescale, surpassing the brilliance of conventional synchrotron sources by eight orders of magnitude. In the year 2005, the Free-electron LASer in Hamburg (FLASH) operated as the first user facility to provide FEL radiation in the XUV regime.

The unprecedented characteristics of FEL radiation open many new possibilities for experiments, but they also come with new challenges to photon pulse diagnostics. The ultra-short time scale and the high photon energy do not allow the usage of many methods that are known for lasers in the optical regime. One of the most challenging parameters to be determined is the duration of the photon pulse. A variety of direct and indirect methods has been proposed for this purpose, but none has yet established itself as a standard.[\[10\]](#)

The present work realizes indirect methods, observing the statistical properties [\[2, 11\]](#) of FEL radiation and considering spectral correlations [\[12\]](#). Each of these methods derives information about the temporal beam profile from the radiation spectra by applying knowledge of the processes within the undulator. Two specific programs were written. One is directly linked to the Data AcQuisition system (DAQ) and gives an estimate of the pulse duration during run time, while the other provides tools for the analysis of previously recorded spectra.

The following chapter contains a brief introduction into the theory of FELs and the processes in the undulator. The following chapters contain theory of the here applied methods for photon pulse length estimation and a description of the experimental set-up as well as of the software tools that were employed for this work. Finally, a selection of measurements is presented and discussed.

Chapter 2

FLASH

FLASH is a single-pass FEL operating in the XUV and soft X-ray regime using Self Amplified Spontaneous Emission (SASE). The basic layout is illustrated in Figure 2.1. A photon pulse from an optical short pulse injector laser hits a photocathode and causes it to emit an electron bunch (RF gun). This bunch is accelerated by a linear accelerator consisting of superconducting cavities up to 1.3 GeV and compressed to a length of some tens of femtoseconds. The accelerated, compressed and collimated electron bunch passes once through the undulator, where the electrons are forced on a sinusoidal path, causing them to radiate photons. After the electrons have passed through the undulator section, a dipole magnet bends the electron beam into a beam dump, while the photon beam is guided through beamlines to the experimental end stations.

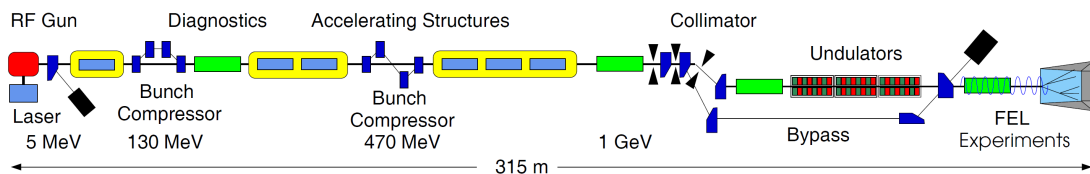


FIGURE 2.1: Schematic layout of FLASH [1]

2.1 SASE - Self Amplified Spontaneous Emission

Let us consider an electron bunch travelling through the undulator, emitting photons due to the sinusoidal path of the individual electrons. After a certain undulator length, the electromagnetic field of the emitted photons becomes strong enough to interact

with the charge distribution within the electron bunch. This causes a process that is known as microbunching, where the density of the overall electron bunch is modulated into several microbunches which are spaced according to the wavelength of the emitted radiation. This process is illustrated in Figure 2.2. Because the longitudinal extension of microbunches is shorter than the wavelength of the emitted radiation, each microbunch emits coherently.

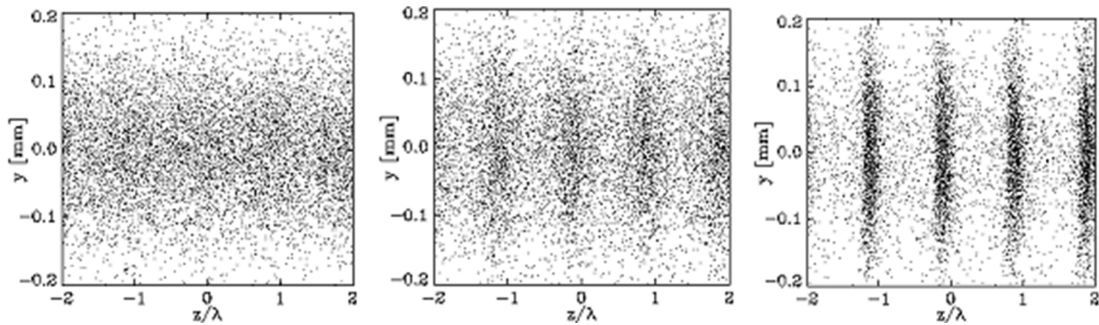


FIGURE 2.2: Example of the development of microbunching along the undulator. The plots show the modulation of the electron density at the undulator entrance (left), within the exponential growth region (middle), and at the undulator exit (right) [2].

Before microbunching occurs, the emitted radiation is incoherent and its intensity is thus proportional to the number of radiating electrons N . However, when the microbunching is complete, the electrons emit photons coherently, causing the power of radiation to grow with the number of radiating electrons¹ N^2 .

Overall, this can be seen as a self-amplification of the radiation within the undulator, giving the process the name Self Amplified Spontaneous Emission (SASE). As the microbunching does not set in directly behind the undulator entrance and can reach saturation before the undulator exit, the radiation of a bunch grows differently depending on the covered undulator distance z .

The graph in figure 2.3 shows the radiation energy of a single photon pulse as a function of undulator distance z and is usually divided into three *undulator regimes*:

1. The regime of spontaneous emission (a). The electrons radiate incoherently, the power of radiation grows linearly.
2. The regime of exponential growth (b). The microbunching has started and causes the power of radiation to grow exponentially².

¹The coherent radiation is only generated by radiating electrons within a single mode. The number of electrons within one mode is in the order of 10^6 to 10^8 .

²If the undulator exit is in this regime, the FEL is said to operate in the *linear regime of operation* (see section 2.1.2), as the corresponding differential Equation has a linear behaviour.

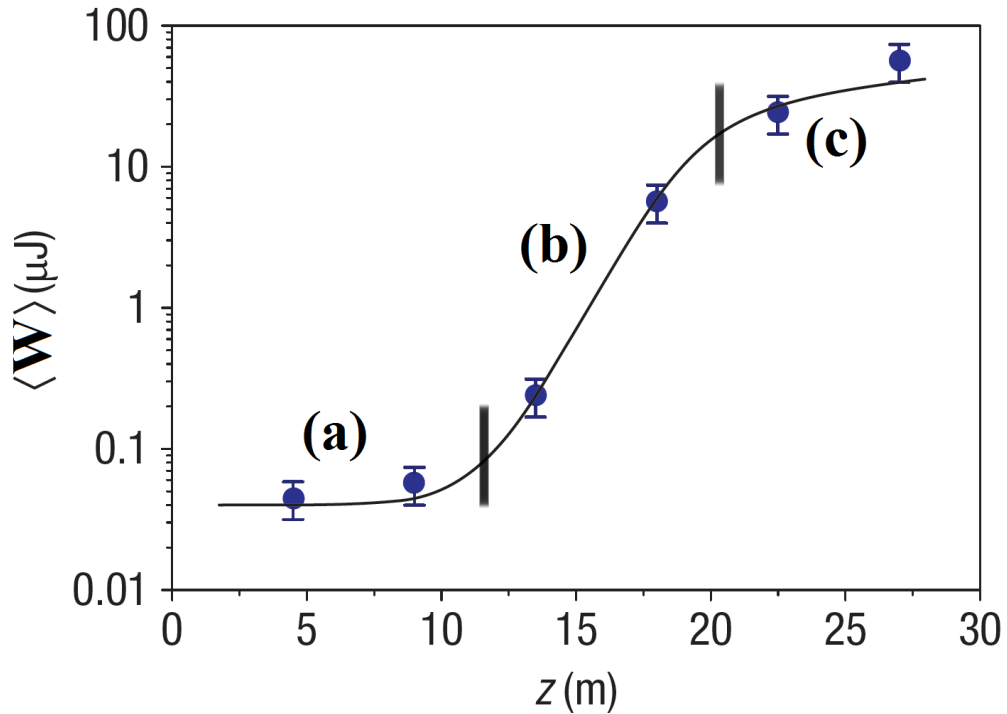


FIGURE 2.3: This undulator gain curve shows the energy in the radiation curve vs. undulator length. The error bars represent the uncertainty of $\pm 15\%$ in the calibration of the detector. [3]

3. The regime of saturation (c). The degree of microbunching does no longer grow.

Further discussion of the SASE-process can be found in reference [13, 14] and the references therein. At FLASH, the fundamental radiation wavelength (see Equation 2.1) can be varied between 4.2 and 45 nm.

2.1.1 The Electron Bunch Shape

For the SASE process to take place at all, a high electron peak current of at least $1 - 2\text{ kA}$ and a low emittance are required. The electron bunch is ejected from the electron gun with a bunch duration of several picoseconds. It is then accelerated by a driving electromagnetic Radio Frequency (RF) wave on a linear path through a number of accelerator modules. In between the accelerator modules, the electron bunch passes through several magnetic chicanes called bunch compressors (See figure 2.1). These lead the electrons of higher energy on a longer path than the ones of lower energy and thereby compress the bunch [3, 9]. The repetition of this process compresses the bunch down to a duration in the order of 100 fs and forms the electron bunch shape. The electron

bunch shape is subject of a sensitive tuning process and therefore varies strongly. It is important to keep in mind that, despite optimization of its parameters, not all parts of the electron bunch contribute to the SASE process.

2.1.2 The two Regimes of Operation

The photons that are emitted by the electrons naturally travel at the speed of light. The electrons however are traveling slightly slower and on a sinusoidal path, so that the emitted photons are traveling ahead of the electrons that emitted them. It is empirically apparent, that the radiation is optimally amplified, if the photon wave emitted by one microbunch is traveling exactly one radiation wavelength λ_r ahead per covered undulator period, so that the next microbunch, located exactly one λ_r ahead of the first, can radiate coherently with the first wave. This so called *slippage effect* leads to the *resonance condition* (see Equation 2.1), which determines the fundamental radiation wavelength. As mentioned earlier, the fundamental wavelength of the emitted radiation is determined by the relativistic factor of the electrons $\gamma = E_{kin}/(m_e c^2)$, the undulator period λ_u and the undulator parameter K [14]. For simplicity, we only consider the wave travelling on the undulator axis.

$$\lambda_r = \frac{\lambda_u}{2 \cdot \gamma^2} \left(1 + \left(\frac{K^2}{2} \right) \right) \quad (2.1)$$

In the undulator regime of spontaneous emission, the degree of microbunching is still small. The photons interact at all locations with the electrons, exchanging energy depending on the relative phase, accelerating and decelerating electrons and thereby increasing the degree of microbunching. The differential radiated intensity increases linearly with the covered undulator distance and the degree of microbunching. The microbunching increases steadily along the undulator until the electron density is optimally modulated with the electrical field of the photons. If the electron bunch exhibits complete microbunching before the undulator exit, the FEL operates in the *saturation regime*; if the microbunching is still in process at the undulator exit, the FEL operates in the *linear regime*.

2.2 Temporal and Spectral Photon Pulse Structure

Considering spatially modulated structure of the electron bunch that is the result of microbunching, we find the temporal structure of the photon pulse to be of a similar nature, exhibiting a number of local maxima which we will refer to as modes. As the modes can be considered to be *Fourier limited*³, their duration corresponds to the coherence time T_{coh} of the radiation. The Fourier limit is reached due to the coherent radiation behaviour of the microbunches. The temporal and spectral structure of the photon pulse are linked by the Fourier transformation. This includes the time-frequency uncertainty, which can be understood as

$$T_{coh} \times \sigma_{\omega} = const \quad (2.2)$$

$$T \times \Omega_c = const. \quad (2.3)$$

Here, T_{coh} is the coherence time (i.e. the duration of a single mode), σ_{ω} is the spectral bandwidth of the overall pulse, T is the overall pulse duration and Ω_c is the degree of spectral coherence (i.e. the width of a single spike in the frequency domain).

This implies that

- the width of the local maxima in the frequency domain Ω_c is inversely proportional to the overall pulse duration T .
- the width of the modes i.e. the coherence time T_{coh} is inversely proportional to the overall bandwidth of the radiation spectrum σ_{ω} .

Figure 2.4 shows qualitative examples for the pulse structure in time and frequency domain.

2.3 Pulse Energy Statistics

The average pulse energy of a FEL pulse depends on the mode of operation. Especially in the linear regime, the Pulse Energy Probability Density Distribution (PEPDD), which describes the normalized probability for an arbitrary FEL pulse to have a total pulse

³An energy chirp of the electron bunch can broaden the modes over the Fourier limit. This effect is discussed in section 3.4.

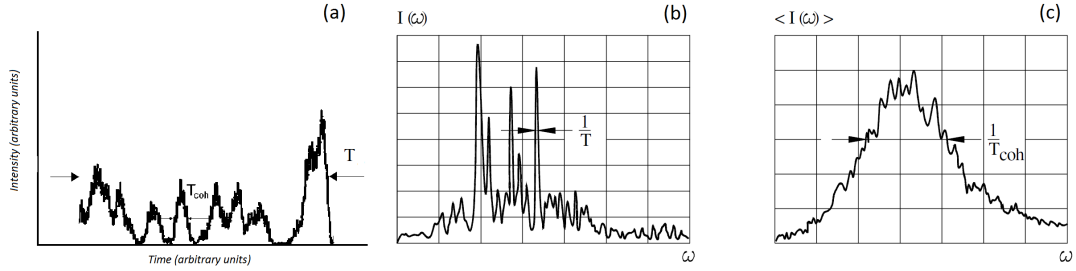


FIGURE 2.4: FEL Photon pulse structure. (a) shows the structure in the time domain. The width of the temporal modes is characterized by the SASE coherence time T_{coh} . (b) shows the structure in the frequency domain. The width of the peaks is inversely proportional to the pulse duration T . (c) shows the structure in the frequency domain, averaged over several shots. The width of the spectrum is inversely proportional to the temporal coherence T_{coh} [4].

energy of W , follows well defined statistics. Figure 2.5 illustrates the PEPDD in different modes of operation.

In the linear regime, the SASE process amplifies each mode individually. The modes originate from shot noise, which follows Gaussian statistics. Due to the large number of electrons within a single bunch⁴ it can be shown using the *central limit theorem* [4] that this causes the number of modes to also follows Gaussian statistics and the PEPDD to follow the gamma distribution [11]:

$$p(W) = \frac{M^M}{\Gamma(M)} \left(\frac{W}{\langle W \rangle} \right)^{M-1} \frac{1}{\langle W \rangle} \exp \left(-M \frac{W}{\langle W \rangle} \right) \quad (2.4)$$

Here, W is the radiation energy of a single photon pulse, M is the *modenumber* and $\Gamma(M)$ is the gamma function. $\langle W \rangle$ represents the average pulse energy within an ensemble.

At the beginning of the saturation regime of the undulator, strong lasing modes become saturated while weaker ones are still amplified. This causes a change of the probability distribution of mode intensities and consequently of the PEPDD. In the saturation regime, the distribution of the energy over the modes does no longer follow Gaussian statistics, but is dominated by non-linear processes. The spectral distribution is broadened and the overall pulse duration increased. The PEPDD does no longer follow a gamma distribution. Consequently, formula 2.4 does *not* hold in the saturation regime. The shape of the PEPDD is now described in [5] as a function of the temporal structure and emittance of the electron bunch as well as of undulator length.

⁴A single bunch can contain about 10^{10} electrons, although not all of them contribute to the sase process.

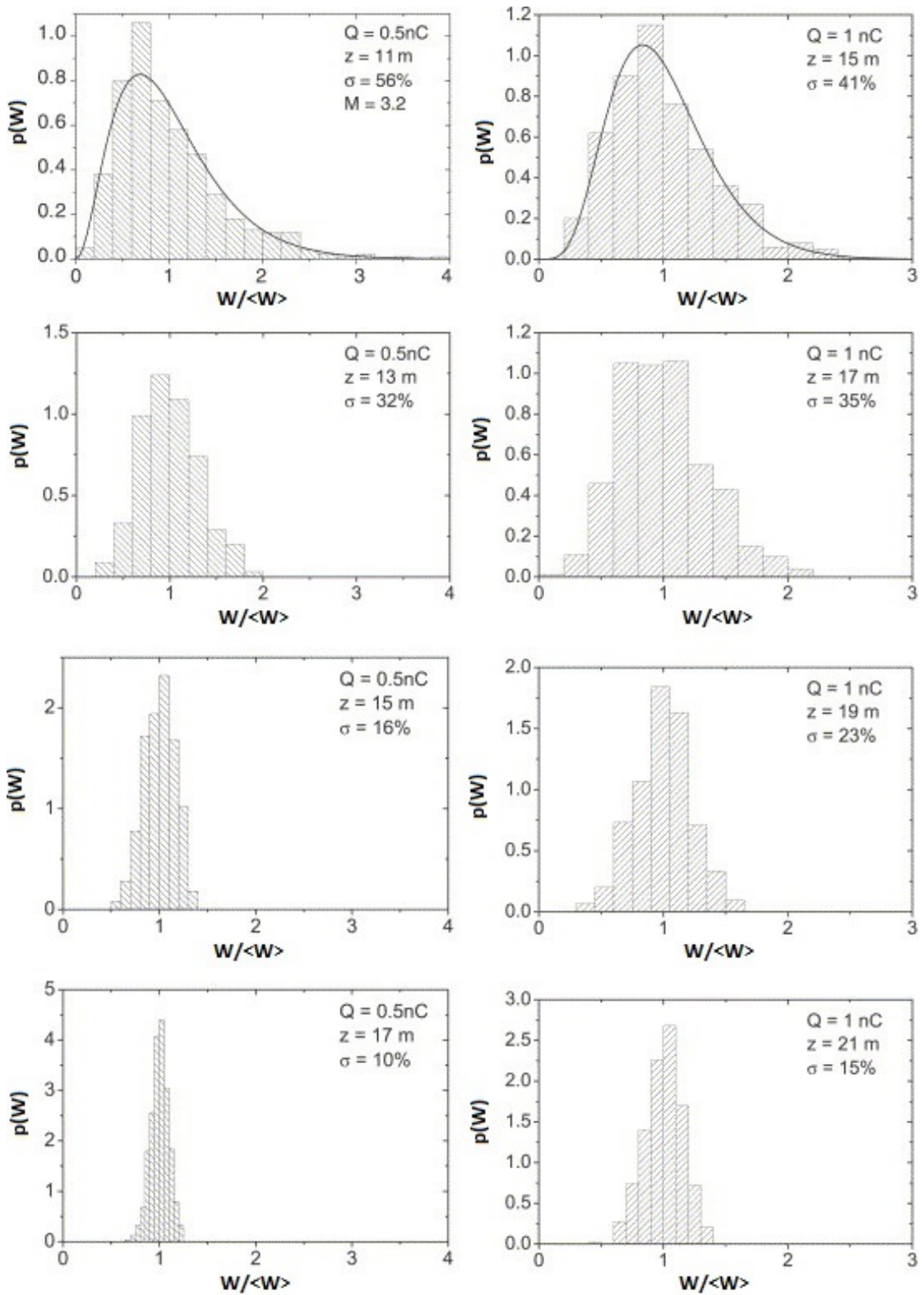


FIGURE 2.5: Evolution of the PEPDD from end of the linear regime down to deep saturation regime, measured in covered undulator distance z . Left and right columns correspond to an overall electron bunch charge of 0.5 and 1 nC, respectively. Solid lines show the gamma distribution. The standard deviation of the PEPDD is given as σ . [5]

Chapter 3

Derivation of the Photon Pulse Duration

Despite its importance for many of the experiments performed at FEL facilities, the reliable determination of FEL pulse duration is still a tremendous challenge. Consequently, a variety of direct and indirect methods have been tested for this purpose [10]. This work mainly concentrates on the second order spectral correlation function, which is an indirect approach using the FEL photon spectra.

In order to make best use of the acquired spectra, two additional methods, the first using the earlier introduced PEPDD and the second employing the number of spectral spikes, are also introduced and realized in this work.

3.1 Spike Counting

A rough estimate of the pulse duration can be achieved by counting the local maxima i.e. *spectral spikes* of the radiation spectra. Considering our knowledge of the photon pulse structure (c.f. section 2.2), it suggests itself that the pulse duration can be estimated as the product of the coherence time T_{coh} and the number of spikes N_ω [10]. This holds true, if the number of spikes in the spectral domain N_ω is similar to the number of maxima in the time domain N_s . Although this approximation is used occasionally, its general validity is not shown for FEL radiation. A more elaborate description of the relation between spectral intensity spiking and pulse duration has been performed by

S.Krinsky and R.L. Gluckstern in [4]. As a more generalized parameter, they observe the number of spikes per unit frequency n_ω . According to [4], this stands in relation to the overall photon pulse length¹ by Equation 3.1. The effects of a possible energy chirp in the electrons as considered in section 3.4 for the second order correlation method have not been investigated for the spike counting method.

$$T = \frac{n_\omega 2\pi}{0.641} \quad (3.1)$$

3.2 Intensity Distribution

A different approach is using the PEPDD and deriving from it the modenummer M . This method differs essentially from the other methods, as only the total energy of each pulse is considered². As mentioned in the previous chapter (c.f. section 2.2), the Pulse Energy Probability Density Distribution corresponds to a gamma distribution dependent on M (see Equation 2.4), if the FEL is operating in the linear regime. Previous works [4] have shown that M is proportional to the number of intensity maxima N_s .

As in the spike counting method, we estimate the photon pulse duration as a product of $N_s \times T_{coh}$.

This consideration leads us to an estimated minimum photon pulse duration σ_{min}^{ph} [10]

$$\sigma_{min}^{ph} \simeq 0.35 \times M \times T_{coh} \quad (3.2)$$

If not specified differently, we will consider the PEPDD of the FWHM part of the FEL photon spectra, although the programmed tools do allow to calculate the PEPDD for any specific, possibly very narrow spectral range within the spectrum³. This can be interesting, for example to observe the suppression of pulse energy fluctuations at ultrashort pulse durations in the saturation regime [5].

¹A flat-top form of the lasing electron bunch was considered.

²Instead of the spectrum.

³This is equivalent to the PEPDD of FEL radiation behind an ideal narrow band monochromator.

3.3 Second Order Correlation

This method compares the second order correlation function computed from measured spectra with the one expected by a theoretical model. Since the spectra themselves originate from a random process, a statistical approach is chosen rather than comparing the spectra directly to a theoretical expected model. This is why the second order spectral correlation is used as a parameter that is unambiguously determinable from both measurement and theory while retaining information about the pulse duration. Figure 3.1 shows such a comparison.

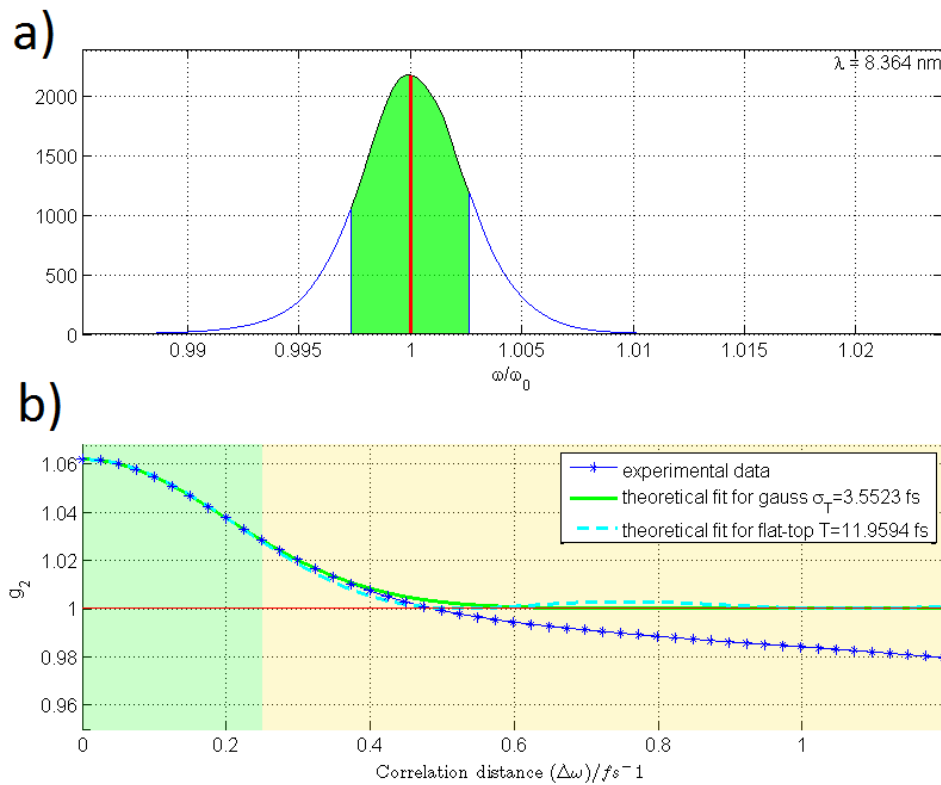


FIGURE 3.1: a) A summation over 395 FLASH radiation spectra. The green area is within the FWHM boundaries.

b) The second order correlation function computed from the spectra with two theoretical fits. The fit parameters σ_T and T represent the rms bandwidth of a Gaussian pulse and the duration of a flat-top pulse respectively. Because the stability of the measured second order correlation function decreases with correlation distance, the fit only regards small correlation distances, underlaid with light green.

3.3.1 Measured Correlation Function

The first and second order spectral correlation are defined as [12]:

$$g_1(\omega_0, \Delta\omega) \equiv \frac{\langle \tilde{E}(\omega_0 - \Delta\omega/2) \tilde{E}^*(\omega_0 + \Delta\omega/2) \rangle}{\sqrt{\langle |\tilde{E}(\omega_0 - \Delta\omega/2)|^2 \rangle \langle |\tilde{E}(\omega_0 + \Delta\omega/2)|^2 \rangle}} \quad (3.3)$$

$$g_2(\omega_0, \Delta\omega) \equiv \frac{\langle |\tilde{E}(\omega_0 - \Delta\omega/2)|^2 |\tilde{E}(\omega_0 + \Delta\omega/2)|^2 \rangle}{\langle |\tilde{E}(\omega_0 - \Delta\omega/2)|^2 \rangle \langle |\tilde{E}(\omega_0 + \Delta\omega/2)|^2 \rangle} \quad (3.4)$$

Where $\tilde{E} = \int_{-\infty}^{+\infty} E(t) e^{i\omega t} dt$ is the spectral electrical field of the laser, ω_0 is the central radiation frequency and $\Delta\omega$ is the correlation distance in the frequency domain. The averaging symbol $\langle \rangle$ represents an ensemble over many bunches and $*$ indicates the complex conjugate.

These must not be confused with the elsewhere known autocorrelation function $A_{ff}(\tau) = \int_{-\infty}^{+\infty} f(x) f^*(x - \tau) dx$. Because of the functions dependence on E and $|E|^2$, some authors also refer to them as field- and intensity-correlation respectively. As a spectrometer is only capable of detecting intensities on its screen, the second order correlation is used. We model a spectrum $S(\omega)$ taken by a spectrometer with a resolution σ_m as:

$$S(\omega) = \int_{-\infty}^{\infty} \frac{e^{-\frac{(\omega' - \omega)^2}{2\sigma_m^2}}}{\sqrt{2\pi}\sigma_m} |\tilde{E}(\omega')|^2 d\omega' \quad (3.5)$$

If we assume the resolution of the spectrometer to be sufficiently narrow that it can be considered to have a shape close to the delta distribution, Equations 3.4 and 3.5 combine to:

$$\lim_{\sigma_m \rightarrow 0} g_2(\omega_0, \Delta\omega) = \frac{\langle S(\omega_0 - \Delta\omega/2) S(\omega_0 + \Delta\omega/2) \rangle}{\langle S(\omega_0 - \Delta\omega/2) \rangle \langle S(\omega_0 + \Delta\omega/2) \rangle} \quad (3.6)$$

This is simply saying that the spectrometer resolution is good enough to measure the spectrum without error. The second order correlation method is described without this approximation in [12].

3.3.2 Expected Correlation Function

In order to assign an expected pulse duration to the measured spectra it arises the need for a theoretical model that describes the expected second order correlation function in dependence of the expected photon pulse duration. The presented model was proposed in previous works [11] and will be shortly introduced at this point.

The idea is that the lasing part of the electron bunch entering the undulator should have the same bunch duration as the photon beam.

The SASE-process starts from fluctuations in the electron beam current $I_e(t)$, as it is passing through the undulator. Therefore we should focus on the statistical properties of this process.

The electron beam current consists of a bunch of N electrons arriving at random times t_k at the undulator entrance and can be described with:

$$I_e(t, t_k) = (-e) \sum_{k=1}^N \delta(t - t_k) \quad (3.7)$$

To describe the form of the electron bunch profile, we introduce a profile function $F(t)$ ⁴, which we will later approximate with ideal Gaussian and rectangular shapes. Using this, we can write the beam current over an ensemble of bunches as:

$$\langle I_e(t) \rangle = (-e)NF(t) \quad (3.8)$$

The probability of an electron arriving in the time interval between t and $t + \Delta t$ if therefore equal to $F(t)\Delta t$.

We can now write the Fourier transform of the electron bunch current:

$$\bar{I}_e(\omega) = \int_{-\infty}^{\infty} e^{i\omega t} I_e(t, t_k) dt = (-e) \sum_{k=1}^N e^{i\omega t_k}, \quad (3.9)$$

And we combine Equations 3.8 and 3.9 into:

⁴The profile function $F(t)$ can be understood as a probability density distribution of the arrival times t_k .

$$\langle \exp(i\omega t_k) \rangle = \int_{-\infty}^{\infty} F(t_k) e^{i\omega t_k} dt_k = \bar{F}(\omega). \quad (3.10)$$

Now we substitute $\omega' = \omega + \Delta\omega$ and consider the first order correlation of the Fourier harmonics $\bar{I}_e(\omega)$ and $\bar{I}_e(\omega')$:

$$g_1 = \langle \bar{I}_e(\omega) \bar{I}_e^*(\omega') \rangle = e^2 \left\langle \sum_{k=1}^N \sum_{n=1}^N \exp(i\omega t_k - i\omega' t_n) \right\rangle, \quad (3.11)$$

and expand it to:

$$\begin{aligned} g_1 &= \langle \bar{I}_e(\omega) \bar{I}_e^*(\omega') \rangle \\ &= e^2 \left\langle \sum_{k=1}^N \exp[i(\omega - \omega')t_k] \right\rangle + e^2 \left\langle \sum_{k \neq n} \exp(i\omega t_k - i\omega' t_n) \right\rangle \\ &= e^2 \sum_{k=1}^N \langle \exp[i(\omega - \omega')t_k] \rangle + e^2 \sum_{k \neq n} \langle \exp(i\omega t_k) \rangle \langle \exp(i\omega' t_n) \rangle, \end{aligned} \quad (3.12)$$

where we find the profile function $F(t)$ in the term $\langle \exp(i\omega t_k) \rangle$ from Equation 3.10, so that we can simplify Equation 3.12 to:

$$g_1 = \langle \bar{I}_e(\omega) \bar{I}_e(\omega') \rangle = e^2 N \bar{F}(\omega - \omega') + e^2 N(N-1) \bar{F}(\omega) \bar{F}^*(\omega'). \quad (3.13)$$

This can be further simplified by considering the case of

$$N |\bar{F}|^2 \ll 1, \quad (3.14)$$

which has been shown to be generally valid within the boundaries of common FEL parameters [11]. Then Equation 3.13 is reduced to:

$$g_1 = \langle \bar{I}_e(\omega) \bar{I}_e(\omega') \rangle = e^2 N \bar{F}(\omega - \omega') \propto \bar{F}(\omega - \omega'). \quad (3.15)$$

It was shown in [11], that when condition 3.14 is fulfilled, the first and second order spectral correlation functions are connected by the Siegert relation:

$$g_2(\omega, \omega') = 1 + |g_1(\omega, \omega')|^2. \quad (3.16)$$

Consequently, we can state for the second order spectral correlation function:

$$g_2(\omega, \omega') = \langle |\bar{I}_e(\omega)|^2 |\bar{I}_e(\omega')|^2 \rangle \propto 1 + |\bar{F}(\omega - \omega')|^2. \quad (3.17)$$

As mentioned earlier, we shall consider the form factors \bar{F} of a Gaussian and a rectangular (flat-top) profile function:

$$\bar{F}_g(\Delta\omega, \sigma_T) = \exp \left[-\frac{\Delta\omega^2 \sigma_T^2}{2} \right] \quad (3.18)$$

$$\bar{F}_{rect}(\Delta\omega, T) = \frac{\sin \frac{\Delta\omega T}{2}}{\frac{\Delta\omega T}{2}}, \quad (3.19)$$

with an rms pulse duration of σ_T for the Gaussian profile form and a duration T for the rectangular profile form. The substitution $\omega' = \omega + \Delta\omega$ was undone here, so that $\Delta\omega = \omega - \omega'$. For these two ideal bunch shapes, we can therefore state the second order correlation functions:

$$g_2^g(\Delta\omega, \sigma_T) \propto 1 + \exp(-\Delta\omega^2 \sigma_T^2) \quad (3.20)$$

$$g_2^{rect}(\Delta\omega, \sigma_T) \propto 1 + \frac{\sin^2 \left(\frac{\Delta\omega T}{2} \right)}{\frac{\Delta\omega^2 T^2}{4}} \quad (3.21)$$

These are the Equations for the second order correlation function that will later be normalized and fitted to the outcome of Equation 3.6, in order to determine the pulse durations σ_T and T .

3.4 Energy Chirp within the Electron Bunch

The second order correlation method is proposed for electron bunches with a uniform electron energy⁵. Real electron bunches however, usually exhibit a temporal chirp of the electron energy within the bunch. This affects the spectral coherence.

Effectively, the second order correlation method measures the degree of spectral coherence Ω_c in order to retrieve the pulse duration. If Ω_c is altered by an energy chirp, the results of the second order correlation method will be affected accordingly. This section discusses that effect on the second order correlation method and proposes an approach to correct for the resulting error.

The here introduced method bases on proposals from [2, 16] and was derived for a flat-top electron bunch form.

As introduced in chapter 2.2, the degree of spectral coherence is inversely proportional to the pulse duration as derived by this method. In the case of a flat-top electron bunch the spectral coherence has been shown [11] to be:

$$\Omega_c = \frac{2\pi}{T} \quad (3.22)$$

However, if the energy of the electrons within the electron bunch is not randomly distributed about a mean value but subjected to a systematic chirp, this causes the degree of spectral coherence to change without a change in coherence time τ_c . This effect has been described in [16] for the case of a linear electron energy chirp over flat-top electron bunch. In this case, the coherence time τ_c is the same for both a chirped and an unchirped electron bunch.

$$\tau_c = \frac{\sqrt{\pi}}{\sigma_\omega} \quad (3.23)$$

The degree of spectral coherence of a photon pulse originating from a chirped electron bunch changes to

$$\Omega_c' = \frac{\sqrt{\pi}|u|}{\sigma_\omega} = |u|\tau_{coh}, \quad (3.24)$$

⁵It is also valid if the electrons are randomly distributed around a constant mean energy [11].

where σ_ω is the SASE gain bandwidth and u is the electron chirp slope parameter as defined in Equation 3.25:

$$|u| = \left| 2 \frac{\Delta\gamma}{\gamma} \omega_0 \frac{1}{\Delta t} \right| \quad (3.25)$$

Further we find [2] that the linear energy chirp causes the bandwidth σ'_ω of the FEL radiation spectrum to stretch with respect to the FEL gain bandwidth σ_ω according to:

$$\frac{\sigma'_\omega}{\sigma_\omega} = \frac{|u|T}{2\sqrt{\pi}\sigma_\omega} \quad (3.26)$$

By dividing expressions 3.24 and 3.22, we obtain:

$$\frac{\Omega'_c}{\Omega_c} = \frac{|u|T}{2\sqrt{\pi}\sigma_\omega} \quad (3.27)$$

We compare Equations 3.26 and 3.27 to arrive at the expression:

$$\frac{\sigma'_\omega}{\sigma_\omega} = \frac{\Omega'_c}{\Omega_c} \quad (3.28)$$

This means, when no systematic chirp is found in the electrons, the bandwidth of the FEL radiation σ'_ω should be equal to the FEL gain bandwidth σ_ω and the measured spectral coherence Ω'_c equal to Ω_c and therefore connected to the pulse duration by Equation 3.22. However if there is a chirp, both photon pulse bandwidth and spectral coherence are increased⁶ by the chirp in the electron energy. The resulting pulse duration from the second order correlation method is inversely proportional to the measured spectral coherence Ω'_c , but the 'real' pulse duration is connected to Ω_c by Equation 3.22. We therefore apply 'chirp-correction' to the pulse duration T_m calculated using the second order correlation method, retrieving the expression for a corrected photon pulse duration T_{corr} :

$$T_{corr} \simeq T_m \times \frac{\sigma'_\omega}{\sigma_\omega} \quad (3.29)$$

⁶The effect can be understood as a 'stretching' of the spectrum.

Chapter 4

The Measurement Setup

All measurements for the purpose of this work were taken at the FLASH facility of the DESY in Hamburg. While most experiments at FLASH require their own unique experiment end-stations, the all measurements in the frame of this work were taken solely with the permanently installed set-up of FLASH. As extensive documentation about the used set-up already exists, this chapter contains but only a short introductions and references to more detailed sources.

4.1 The PG Monochromator Beamline

All the methods described in the previous chapter require high resolution photon pulse spectra of the FEL beam. These spectra were taken at the Plane Grating (PG) monochromator beamline. This beamline is permanently installed in the FLASH experimental hall and is capable to function either as a monochromator or as a spectrometer. In this work, the beamline was always operated in spectrometer mode. It follows a brief description of the beamline setup and the general parameters. For more detailed information about the beamline, please see [6, 9].

Figure 4.1 shows schematic views of the beamline from a vertical and a horizontal perspective. In the Figure, the photons, illustrated by the yellow beam path, are entering from the left. The first mirror M0 is a plane switching mirror. By adjusting this mirror, the active photon beamline can be selected. M1 is a toroidal mirror which focuses the beam onto the intermediate focus Z. M2 is another plane mirror and functions as a

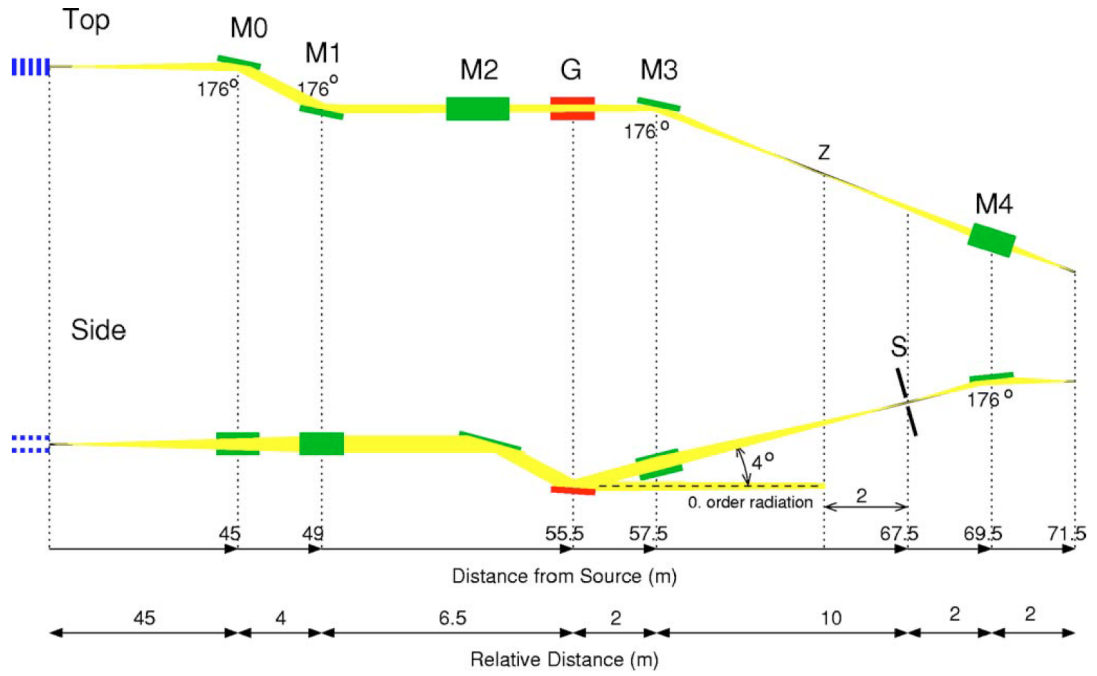


FIGURE 4.1: Schematic layout of the PG2 monochromator beamline at FLASH. The mirrors M0 to M4 are indicated in green, the plane grating G in red. The exit slit S can be replaced by a Ce:YAG screen for spectrometer mode. [6]

Optical element	Distance from source [m]	Deflection angle	Shape	Radius [m]	Size [mm^2]	Slope error
M_0	45	4°	plane		40×490	0.1''
M_1	49	4°	toroidal	714.8/3.63	30×490	0.5''
M_2	55.4	$2 - 16^\circ$	plane		20×490	$< 0.1''$
Grating*	55.5	$2 - 16^\circ$	plane		30×200	$< 0.1''$
M_3	57.5	4°	sagittal	0.698	30×280	0.5''
Slit	67.5					
M_4	69.5	4°	toroidal	57.3/0.093	20×230	0.5''
Focus PG2	71.5					

* 200 lines mm^{-1} grating: depth of groove 35nm, groove width 0.65 measured on top, 1200 lines mm^{-1} grating: depth of groove 10nm, groove width 0.66 measured on top.

TABLE 4.1: Parameters of the optical elements of the beamline according to Figure 4.1. Table from [9].

premirror to the grating G. Together they form the Mirror Grating Unit (MGU). Mirror and grating can be moved together, thereby changing the incident angles of the beam onto premirror and the grating while keeping the position of the focus constant. This is described by the fixed focus constant c_{ff} , which is the quotient of the sines of the angles of incident and diffraction.

$$c_{ff} = \frac{\cos \beta}{\cos \alpha} \quad (4.1)$$

By varying the c_{ff} value, the spectrometer resolution and order of diffraction on the spectrometer screen can be changed. The MGU is illustrated schematically in Figure 4.2.

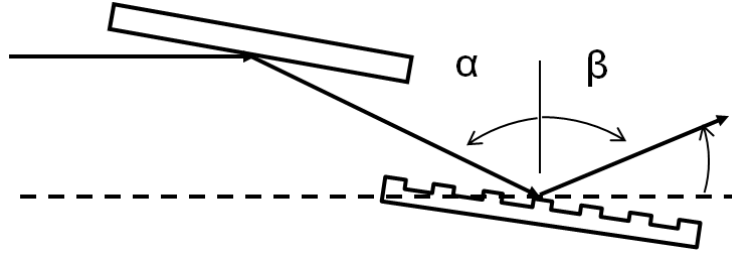


FIGURE 4.2: Schematic view of the MGU, consisting of the grating G and the premirror M2. Indicated are the angles of incident α and diffraction β .

Depending on the c_{ff} value, the diffracted light of first or higher order passes on to the M3 mirror, while the zeroth order diffraction light can pass on to the PG0 beamline, which we will not discuss here. The M3 mirror has a sagittal form and focuses the beam in the horizontal plane onto the exit slit S. When the beamline is operated in spectrometer mode, the exit slit is replaced by a Ce:YAG crystal¹. The crystal serves as a screen and is imaged by a Nikkor fast macro lens with 1:1 magnification onto a triggered fast shutter Intensified CCD camera². The beamline uses the camera model ANDOR iStar DH740. This If the beamline operates in monochromator mode, the monochromatic beam is refocused by the M4 mirror onto a sample or experimental end-station.

The geometric details of the components are shown in table 4.1. All mirrors have been coated with amorphous Diamond Like Carbon by the GKSS research centre in Geesthacht for optimizing reflectivity. Not shown in Figure 4.1, a Water-cooled Aperture Unit (WAU) is inserted between M1 and M2. The WAU provides two freely adjustable slit-apertures, one in the horizontal and one in the vertical direction. The apertures are water-cooled to avoid overheating at high FEL intensities. The PG beamline is thoroughly investigated in [9] and the references therein.

¹1% Ce content, spatial resolution better than $10\mu m$, maximum of scintillation intensity at about $550nm$ [9].

²The spacial resolution of the intensifier tube is $30\mu m$, the effective pixel size of CCD chip amounts to $13.5\mu m$, the quantum efficiency at $400nm-600nm$ is about 50% [9].

4.1.1 Tilt of Spectral Lines on the Spectrometer Screen

Another effect that has been observed during our measurements was a tilt of the spectral lines on the spectrometer screen, as it can be seen in Figure 4.3. This effect does not indicate poor beamline alignment but occurs when the FEL is not optimally tuned. However the exact reason for the effect is not known to us.

Considering the image on the camera screen as shown in Figure 4.3, the intensities recorded by the camera are integrated along the y-axis and projected onto the (dispersive) x-axis³. If the spectral lines have their usual orientation parallel to the y-axis of the Figure, this generates an optimal spectrum. If however the spectral lines are tilted as in Figure 4.3, the projected spectrum will be 'smeared out' along the dispersive axis.

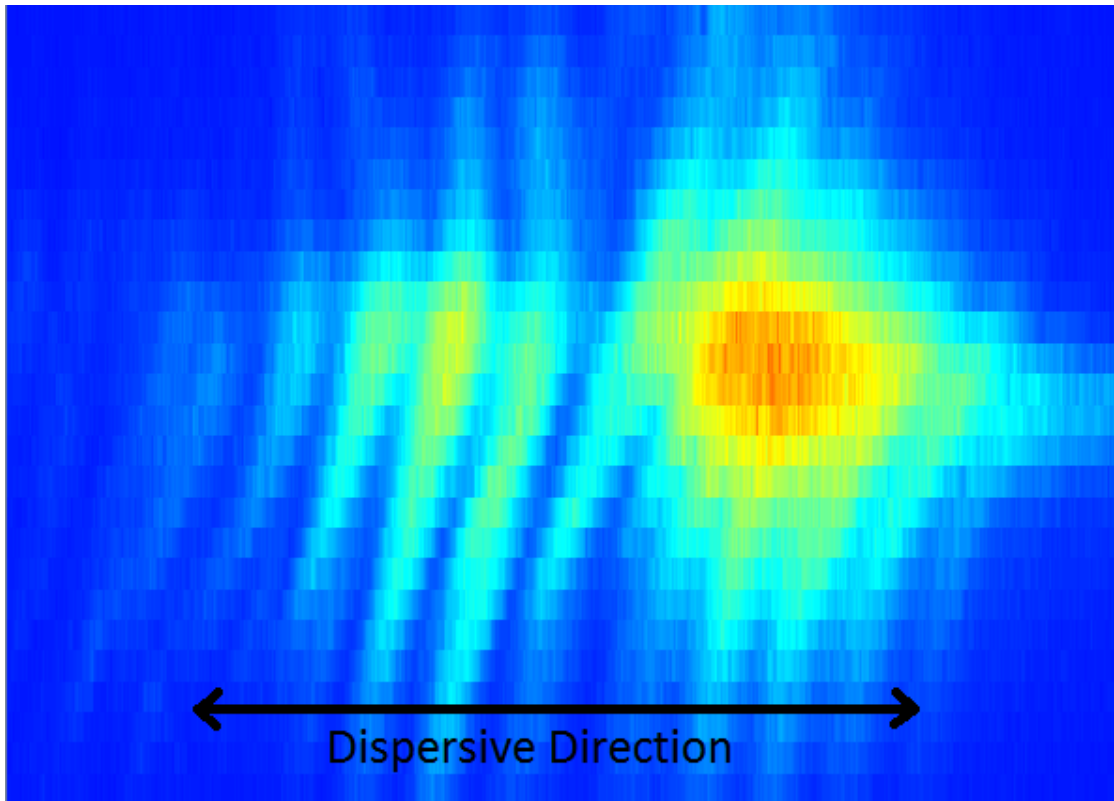


FIGURE 4.3: A plot of the unaltered camera image from the end of the PG monochromator beamline. We observe a tilt of the spectral lines.

The effects on the pulse duration measurement are similar as those of an electron energy chirp. The affected spectrum appears to have a larger spectral coherence and therefore a shorter pulse duration. However in this case, the spectral bandwidth is not affected.

³The x-axis in Figure 4.3 corresponds to the vertical orientation of the beamline. The physical orientation of the camera is turned by 90° with respect to the orientation of the Figure.

Unfortunately the reasons for this tilt are not well understood and we can therefore not correct for the effect.

An additional difficulty is that the mentioned projection process is computed within the cameras evaluation server and the direct image is usually not saved to the DAQ.

The chosen approach to this problem is to neglect the projection and instead consider a selected single horizontal line. This prevents the spectrum from smearing out, but at the same time restricts the measurement to a slim slice of the beam and makes it sensitive to a beam position jitter. The single line spectra are therefore only used for the second order spectral correlation method, as it is most sensitive to changes in the spike width. In the measurements chapter, 'whole beam' spectra refer to a projection of the non-dispersive axis onto the dispersive one, while 'single line' spectra are the intensities on a single line⁴ along the dispersive axis.

4.2 Transverse Deflecting Structure LOLA

At FLASH, the longitudinal electron bunch structure can be analysed using the Transverse Deflecting Structure (TDS) LOLA⁵. As detailed documentation exists in [8, 15, 17] and would exceed the frame of this work, this section is restricted to explaining the general functionality of the TDS set-up.

The TDS can linearly transfer the longitudinal structure of the electron bunch into a transversal structure by subjecting the bunch to the streaked electromagnetic field of a RF wave running in parallel to the flight direction of the electrons. This principle is illustrated in Figure 4.4.

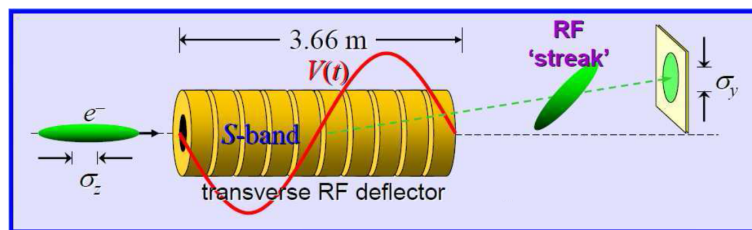


FIGURE 4.4: Working principle of the transverse deflecting structure LOLA. The longitudinal electron bunch profile is streaked by a RF wave and thereby converted into a transverse structure that is detectable on a projection screen. [7]

⁴The camera server uses vertical binning. The extension of the line in the non-dispersive direction is therefore variable.

⁵Named after its designers G. LOew, R. Larsen and O. Altenmueller.

LOLA is set up directly upstream the undulators and can run in dispersive or non-dispersive mode. In non-dispersive mode a fast kicker magnet behind the actual TDS redirects a single bunch out of the bunch train onto one of two camera screens, thereby capturing the longitudinal bunch structure. Non-dispersive LOLA measurements can be performed in parallel to FEL operation. In dispersive mode, the vertically streaked electron bunch is directed through a dipole magnet that deflects the electrons horizontally with a deflection angle depending on their energy, effectively generating an energy dispersion in the electron bunch. When this bunch is projected on a camera screen, this results in a phase space measurement, as the temporal i.e. longitudinal structure is resolved on the vertical axis while the electron energy is resolved on the horizontal axis. In a non-dispersive measurement, the set-up resembles a streak camera for electron beams. A dispersive measurement additionally resolves the spectral information orthogonal to the streak direction.

Because the dipole magnet can not be switched on and off quickly enough to select a single electron bunch from the bunch train⁶, dispersive measurements can not be done in parallel to FEL operation.

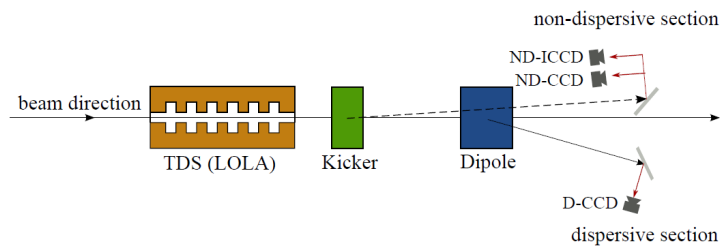


FIGURE 4.5: A simplified schematic of the TDS LOLA at FLASH. Quadrupole magnets are neglected for simplicity. [8]

⁶Ramping up the dipole magnet requires several minutes during which FEL operation is not allowed.

Chapter 5

Developed Evaluation Software

In order to perform the pulse duration measurement as described in chapter 3, two specific applications have been developed. This chapter introduces their purpose and shows the process of a complete example measurement, utilizing all provided methods and tools. All MATLAB scripts were developed in the frame of this work¹ and are published as full code in [18].

5.1 Developed Applications

As mentioned earlier, one of the most outstanding advantages of this method for photon pulse length determination is the quick availability of the required data in form of the radiation spectra. The photon pulse duration is a very important parameter in many other experiments and is often required before or during the experiment, requiring the evaluation to be fast. At the flash facility, all measurements are sent to a Data Acquisition system (DAQ), which pre-processes the measurement data in so called middle layer servers² and then stores them to a central file storage system. Usually, experiment evaluation is done by downloading the records from the file storage and evaluating them locally. This has many advantages, as the original data is not lost and is available to any number of scientists for a long time. For the evaluation of these recorded data, the

¹Some of the scripts base on algorithms developed by Svitozar Serkez for [2]. Also, some public non-standard MATLAB functions were used. The latter are indicated and referenced in the function headers.

²A middle layer server functions as a permanently running instance in the DAQ, evaluating any recorded data instantly.

Statistic Spectra Analysis (SSA) GUI has been programmed as a MATLAB application. This application provides many tools for a detailed spectra analysis. However, the SSA GUI requires a manual download of a specified set of spectra from the DAQ and does not provide a quick and direct measurement method. That is why the evaluation algorithm has also been implemented as a middle layer server, processing the recorded spectra in real time and producing measurement results with a delay of seconds. This server is running under the name Photon Pulse Length (PPL) server.

5.2 Example Measurement

This section shows one measurement procedure, using all essential parts of the developed software. The methods are presented in a reasonable order but can be performed individually and independently at any time and order³.

5.2.1 Dispersed TDS Measurement

If the second order correlation method is to be used in a measurement, it is recommendable to determine the SASE gain bandwidth for the current FEL settings using the Transverse Deflecting Structure (TDS) LOLA.

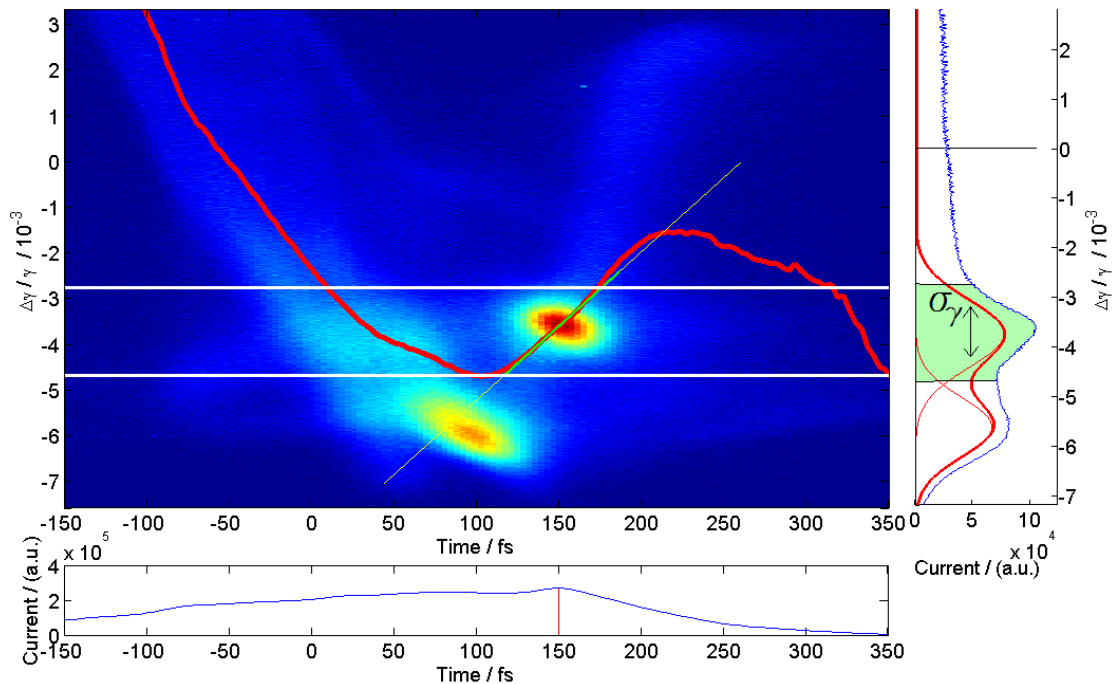


FIGURE 5.1: Dispersed LOLA measurement taken at 05.09.2015, 15:49. In the particular measurement shown in this Figure, the electron bunch exhibits two maxima in the phase space, which is a result of non-optimal FEL tuning. As our theoretical model does not cover the case of multiple maxima, the weaker maximum has been neglected and the Gaussian fit to the higher maximum has been used for the measurement. The estimated relative SASE gain bandwidth with electron chirp amounts to 0.452% FWHM.

As the electron bunch serves as the "gain medium" in a Free Electron Laser, the gain bandwidth can be calculated by measuring the spectral bandwidth of the lasing electrons.

³The dispersed TDS measurement should be taken at a similar time as the spectra and evaluated first, if the result is used for the second order correlation method.

For this, a dispersed⁴ LOLA image has to be taken. Such an image is shown in Figure 5.1. The energy distribution is then fitted by a Gaussian fit and the corresponding rms relative frequency bandwidth σ_ω/ω , which is a measure for the relative SASE gain bandwidth, is computed from the fit parameters according to Equation 5.1, which was derived for this purpose by Svitozar Serkez in [2].

$$\frac{\sigma_\omega}{\omega} = 2 \frac{\sigma_\gamma}{\gamma} \quad (5.1)$$

This is compared to the average bandwidth σ'_ω of the recorded spectra, resulting in the correction factor $\sigma'_\omega/\sigma_\omega$ for the electron chirp. If a dispersed TDS measurement is not available for any measurement set, a standard relative SASE gain bandwidth of 0.4% FWHM can be used as an approximation.

⁴For a dispersed image, both the time and energy distributions of the bunch are measured. See chapter 4.2.

5.2.2 PPL-Server Measurement

The Photon Pulse Length server was created to enable a real-time feedback on the photon pulse duration. It has been included into the Photon Beam Diagnostics DAQ and automatically evaluates any recorded spectra using the second order correlation method. The control panel of the server is shown in Figure 5.2.



FIGURE 5.2: Control panel of the Photon Pulse Length server. The plots on the left show the input spectra (up to down) directly from the camera, after the low-pass filtering and the accumulated spectrum over the last 300 spectra. The plot to the upper right shows the calculated second order correlation function including the fits for Gaussian and flat-top electron bunches. The measurement result for the Gaussian electron bunch shape, averaged over the last 50 calculations and corrected for electron bunch chirp is displayed to the lower right, including the standard deviation. Measurement taken at 05.09.2014, 17:30.

The control GUI displays the direct estimate of the currently measured average⁵ photon pulse duration and shows plots of the second order correlation function and the input spectra. Separate tabs provide some additional information about the measurement and a number of control parameters can be specified. For more detailed information about the PPL server, see [19].

⁵The displayed value is the average result of the last 50 calculations.

5.2.3 Extracting Spectra from the DAQ

If the results from the PPL server are not detailed enough, it is possible to evaluate the recorded spectra off-line using the SSA MATLAB tool.

This requires a download of the respective spectra from the DAQ storage using the `SaveDAQdata`⁶ script. It has to be executed from `flashlxuser1`, or another machine in the DESY network on which the MATLAB extension `daq_read_svr` is installed. The script requires the user to specify the required spectra in the form of a `.xml` file, which can be created using the DOOCS Java application `DAQdataGUI` [20].

An alternative way to download the spectra is using the DOOCS Java application `DAQdataGUI-experimental` [20] to save the spectra in form of a text file. However this way is not recommended, as it is more sensitive to errors and the association of the spectra with their event ID⁷ will be lost.

⁶See Appendix A.

⁷The event ID is used by the DAQ in order to attribute the correct recording time to each pack of data.

5.2.4 Starting the SSA MATLAB GUI

If the file with the spectra is successfully saved, it can be read into the SSA MATLAB GUI. To start the SSA GUI, execute the script `RunGUI`⁸.

The `RunGUI` script will directly open the file selection for a spectra file⁹ and load the selected file into the SSA GUI, which is pictured in Figure 5.3.

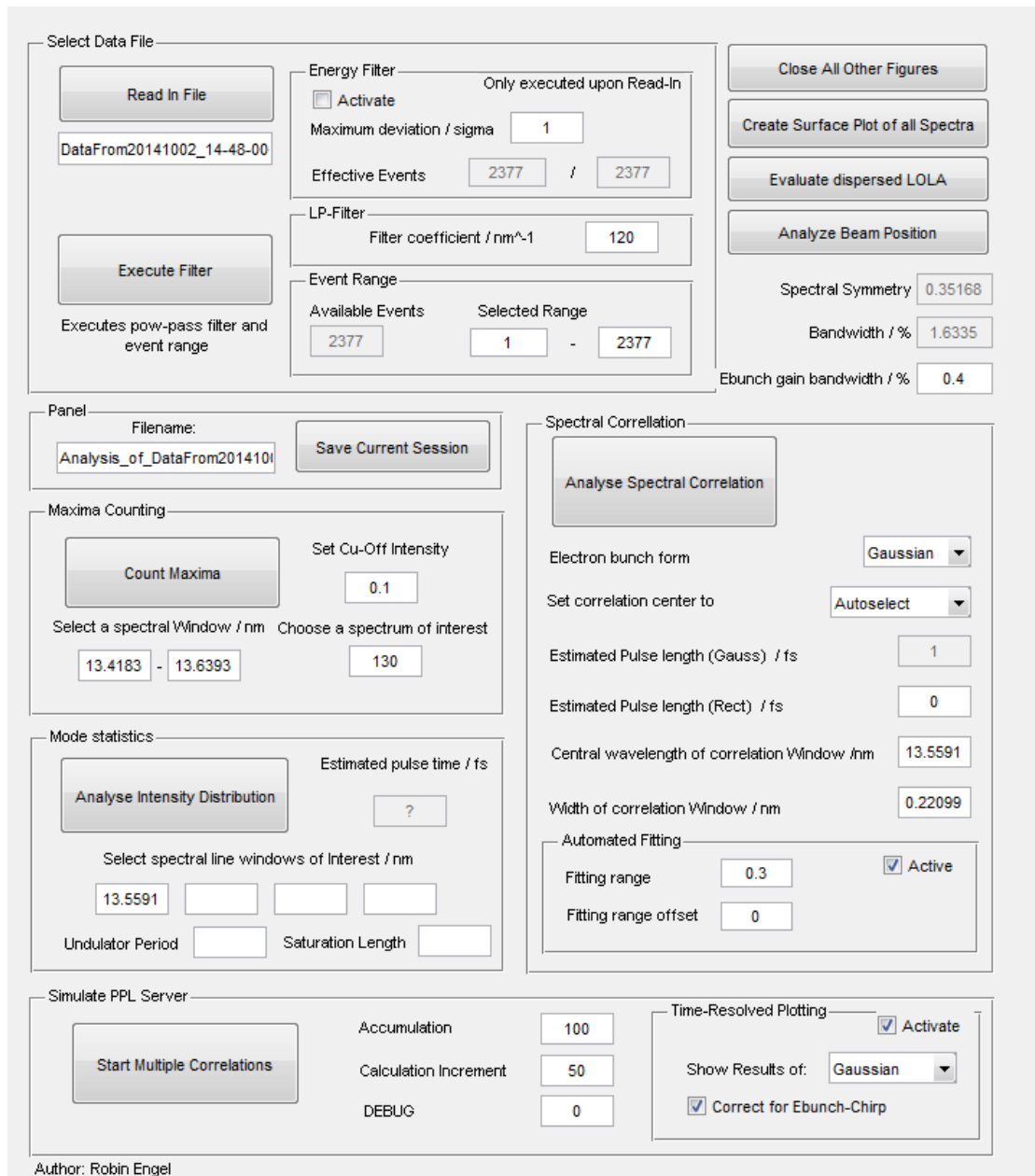


FIGURE 5.3: Picture of the Statistic Spectra Analysis GUI.

⁸At this point it is important to make sure that all function files of the SSA GUI as well as the loaded data file are included in the active MATLAB path.

⁹Either in the `.mat` or `.txt` format, selectable in the bottom right corner.

5.2.5 Spectra Overview

In order to get a first overview of the loaded spectra, a plot of the complete set can be created with the button **Create Surface Plot of all Spectra**. This can be helpful to get a general impression of the recorded spectra.

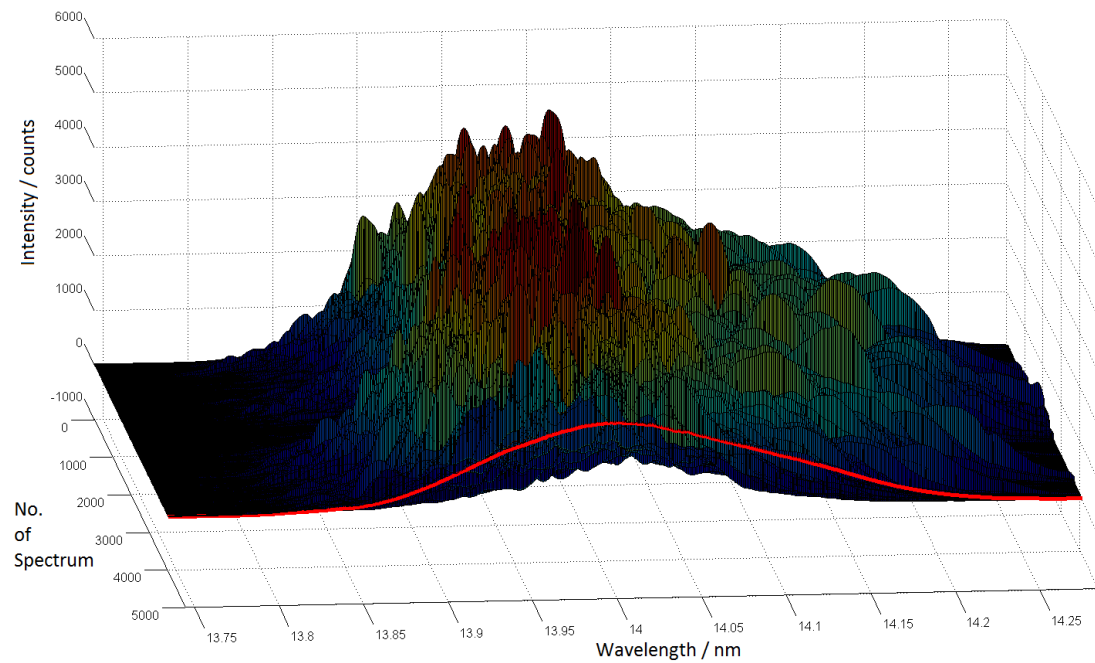


FIGURE 5.4: An overview plot of 4053 Spectra. The red line represents the average spectrum. The Measurement taken at 05.09.2014, 18:49.

5.2.6 Setting Filters

Before the spectra are passed to the evaluating algorithms, a low-pass filter¹⁰ with a freely selectable cut-off frequency is applied to remove camera noise. The effect of the filter and its cut-off frequency has been studied in [2]. The default cut-off frequency is $120/nm$.

If for any reason not all spectra should be considered in the evaluation, the active event range can be freely selected.

Another possibility to preselect the spectra is the energy filter. This filter considers the shot energy¹¹ of each spectrum and compares it to the average shot energy. If a selectable multiple of the standard deviation of all shot energies is exceeded, the respective event will not be considered.

All three filters are executed upon pressing the button **Execute Filter**.

¹⁰The low-pass filter works by calculating the Fourier-transform of the spectrum, removing all frequencies that exceed the cut-off frequency and transforming the spectrum back afterwards. The MATLAB code is published in [18].

¹¹Computed by integrating the spectral intensities over the full spectrum.

5.2.7 Spike Counting

The spike counting method can be applied with the button **Count Maxima**. The algorithm filters the spectrum with the low-pass filter described in section 5.2.6 and additionally removes any spectral intensities that are smaller than a selectable fraction I_{\min} ¹² of the maximum spectral intensity. This filtering is illustrated with a selectable example spectrum in the output plot, as shown in Figure 5.5. After filtering, an algorithm counts all remaining local maxima, thereby distinguishing between those within and without the FWHM part of the spectrum. The number of spikes is then plotted against the event number of the respective spectrum; the red line represents an average over the last 100 events. The calculated average photon pulse duration calculated according to Equation 3.1 is displayed in the command window, as well as number of spikes per spectrum, per FWHM and per unit frequency. The algorithms used by this function are derived from those developed by Svitozar Serkez for [2].

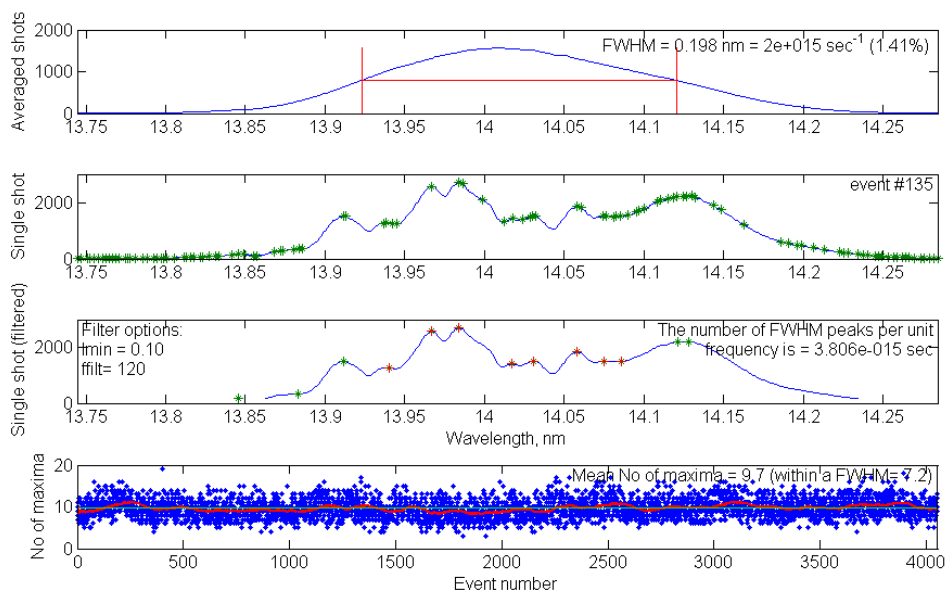


FIGURE 5.5: Plot generated with the **Count Maxima** button. The plots show (up to down) the average spectrum of all considered spectra, a selected example spectrum before filtering, the same example spectrum after filtering and the number of spectral spikes within the whole spectrum over the event index. Measurement taken at 05.09.2014, 18:49.

¹²Usually, I_{\min} is set to 0.1.

5.2.8 Intensity Distribution

A spectra analysis by intensity distribution statistics (PEPDD) is performed upon pressing the button `Analyze Intensity Distribution`. By default, the PEPDD is computed for the FWHM window around the central frequency. It is however possible to specify up to four discrete wavelengths of interest, for which the PEPDD and respective M-values will also be calculated. In the example shown in Figures 5.6 and 5.7, the central wavelength of 14.0063nm and as a wavelength of interest, 14.1500nm were specified as line window locations. The FWHM window ranged from 13.9229nm to 14.1206nm .

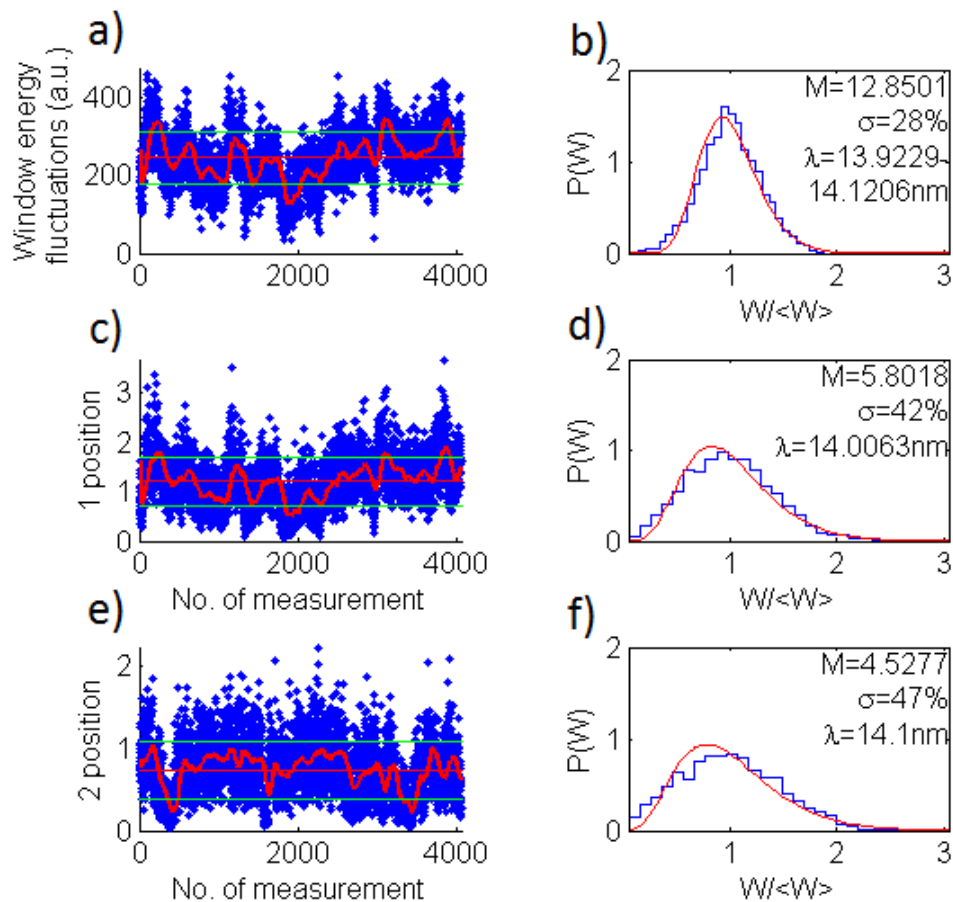


FIGURE 5.6: First plot generated with the `Analyze Intensity Distribution` button. The left column shows the development of pulse energy within the FWHM window (a) and the line windows (c) and (e) around the two selected frequencies. The right column shows the measured and calculated PEPDD for the same spectral windows. Measurement taken at 05.09.2014, 18:49.

Figure 5.6 shows the spectral intensity statistics. The first plot (a) shows the pulse energy within the FWHM window; in (b), the blue bar-plot represents the measured

probability density and the red fit is the expected curve calculated with Equation 2.4. Plots (c) to (f) are calculated accordingly, but in their case only the line window at exactly the specified wavelength is considered. To understand the plots of Figure 5.6 better, one might imagine summing up the plots of the left column along their x-axis. If one normalizes the resulting distribution to a unit area, this will yield the PEPDD that is shown as blue bar plots in the right column.

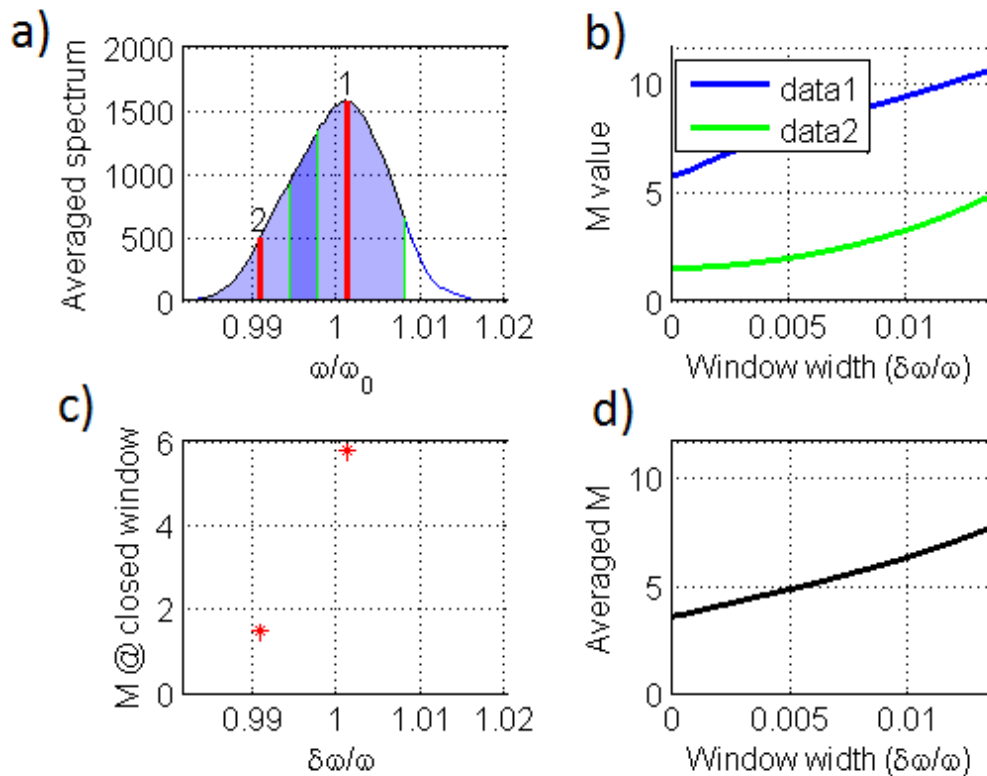


FIGURE 5.7: Second plot generated with the **Analyze Intesity Distribution** button. Plot (a) illustrates the selected windows in the averaged spectrum, plot (b) shows the M-values of frequency windows around the selected wavelength with a variable window width. Plot (c) shows the M-Values of the line windows marked in (a) at their respective relative frequency and (d) shows the averaged curve of the ones displayed in (b). Measurement taken at 05.09.2014, 18:49.

As demonstrated in Figure 5.6, an M-Value can be computed for a frequency window of arbitrary location and width. As Figure 5.6 only covers three specific windows, Figure 5.7 shows the calculated M-values for different widths of the frequency window. The central frequencies around which the windows are computed are those of the line windows specified before. Plot (a) illustrates the selected windows in the averaged spectrum, plot (b) shows the M-values of frequency windows around the selected wavelength with a

variable window width, up to a maximum width that is marked blue in (a). Plot (c) shows the M-Values of the line windows marked in (a) plotted over their respective relative frequency and (d) shows the averaged curve of the ones displayed in (b). This simulates the measurement of M values behind a monochromator of variable bandwidth.

When the FEL is operating in the saturation regime, this evaluation can not be used to derive information about the photon pulse duration.

The core algorithms used in this intensity distribution analysis those developed by Svi-tozar Serkez for [2] and have been integrated into the SSA GUI. They provide the user with a M-Values for different parts of the spectrum. Although [2] suggests the FWHM window for the pulse duration estimation according to Equation 3.2, no further investigation on the influence of the selected frequency window was done in this work.

5.2.9 Single Second Order Correlation Run

This function applies the second order correlation method to all loaded spectra at once. Figure 3.1 shows the created plots. The second order correlation function is computed from the spectra using Equation 3.6 and fitted with Equations 3.20 and 3.21 by a least squares algorithm. The user can select a number of parameters to optimise the measurement. These are:

- The `Electron bunch form` menu controls if either one or both electron bunch forms should be considered. It is well to keep in mind that the parameter for a Gaussian shape is the rms duration, while the parameter for a flat-top form is the overall duration, which is about a factor of $\sqrt{12}$ longer.
- The `central wavelength` around which the correlation is calculated is by default the expected value of the spectrum. In case of a very asymmetric set of spectra, the `Autoselect` option switches to the wavelength of maximum intensity. This can also be done manually. Alternatively, the central wavelength can be entered manually.
- The `Automated Fitting` can be activated or deactivated by a check-box. If it is deactivated, the theoretical fits will not be optimized by the least squares fit, but just be potted according to the selected values.

- The `Fitting range` and `Fitting range offset` control the maximum range of correlation that is considered by the least squares process. The `Fitting range` is the considered fraction of the difference between maximum of the second order correlation function and one. It can be varied between 0 and 1, but usual values are 0.1 to 0.5. The `Fitting range offset` is a fixed number of data points that should additionally be considered. It can be any integer number.

When this function is used it is important to keep in mind that the displayed results are the direct fit parameters for Equations 3.20 and 3.21. That is the pulse duration for a flat-top bunch and the rms pulse duration of a Gaussian bunch, both neglecting effects of a possible electron chirp. Previous works [12] have shown that the ratio between both is usually $T/\sigma_T = \sqrt{12}$.

5.2.10 Multiple Second Order Correlation Run

Generally, a larger set of acquired spectra delivers a more accurate estimation of the second order correlation function and therefore the pulse duration. However there are several reasons why it can be interesting to break up the original set of spectra into many smaller ones.

One reason are machine instabilities within the measurement period. It has been shown in [2], that a fluctuation of the photon energy (i.e. wavelength) can have a strong negative influence on the measurement. As such fluctuations usually happen on a relatively slow time scale, the effect of the fluctuations can be reduced by considering smaller sets of spectra¹³.

Another reason is the possibility to observe the development of the photon pulse duration over the measurement period. Lastly, the multiple calculation can give an impression of the unsystematic error of the method. If FEL parameters are constant over the measurement period, the obtained distribution of results exhibits a standard deviation equal to the unsystematic error. In a real measurement, the standard deviation additionally contains the real fluctuations of FEL pulse duration. Systematic errors can not be estimated by this approach.

¹³Which were each recorded within a short period of time.

The number of spectra considered in each calculation can be set using the `Accumulation` parameter, the `Calculation Increment` controls the increment between measurements. This function uses the same algorithms that are used by the PPL server. Its results are therefore not presented as fit parameters. Instead they already contain the correction for electron chirp and the Gaussian pulse durations are displayed in FWHM. The fit range used for the least squares fit is the one specified in the section for the single second order correlation function.

The resulting plot is shown in Figure 5.8. Additionally, the second order correlation function of every partial measurement is calculated and plotted similarly as for the single second order correlation function.

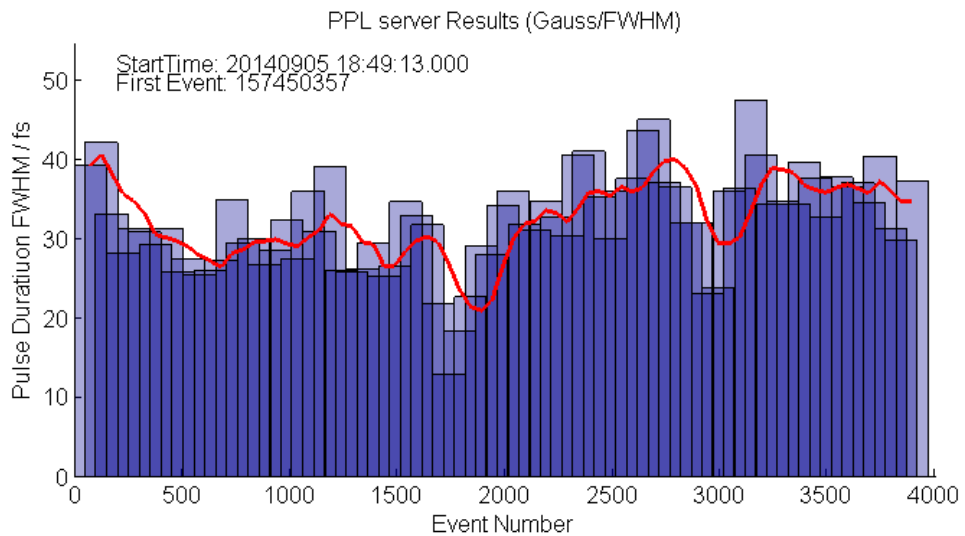


FIGURE 5.8: Result plot of a multiple correlation run. Each bar represents one measurement. The red line is the averaged pulse durations. In this case, each measurement used a set of 150 spectra with an increment of 50 spectra. The Plot also shows the DAQ event ID and exact time of the first spectrum.

Chapter 6

Measurements

In this chapter, a number of measurements performed with the introduced methods and software will be presented. The results of the alternative methods will be compared to each other and to measurements of the electron bunch taken with the TDS LOLA. We have performed a number of measurements under variation of different parameters in order to determine the influence of the respective parameters on the results and the reliability of the method.

One of the biggest challenges within this work is the estimation of the measurements accuracy. The experimental outcome is dependent on many parameters. Up to now the influence of the different parameters on the pulse length measurement is not investigated in detail. The measurements in this chapter are concerned with the determination of these dependencies. However, as the multiple second order correlation method offers a number of results for each measurement, their standard deviation can serve as inherent error and is shown in form of error-bars in some plots. It is important to keep in mind that this does not cover systematic errors¹.

¹As such from non-Gaussian lasing bunch form, varying electron gain bandwidth, manipulation of the photon beam etc..

6.1 Comparison and Temporal Stability

As the verification of the here developed methods by other photon pulse duration measurements could not be performed in the frame of this work, the best approach is the comparison of the different methods, that were realized in this work, to each other. In this section, we see a comparison of the spike counting and second order correlation methods. Additionally, we plot the fluctuations in the overall pulse energy.

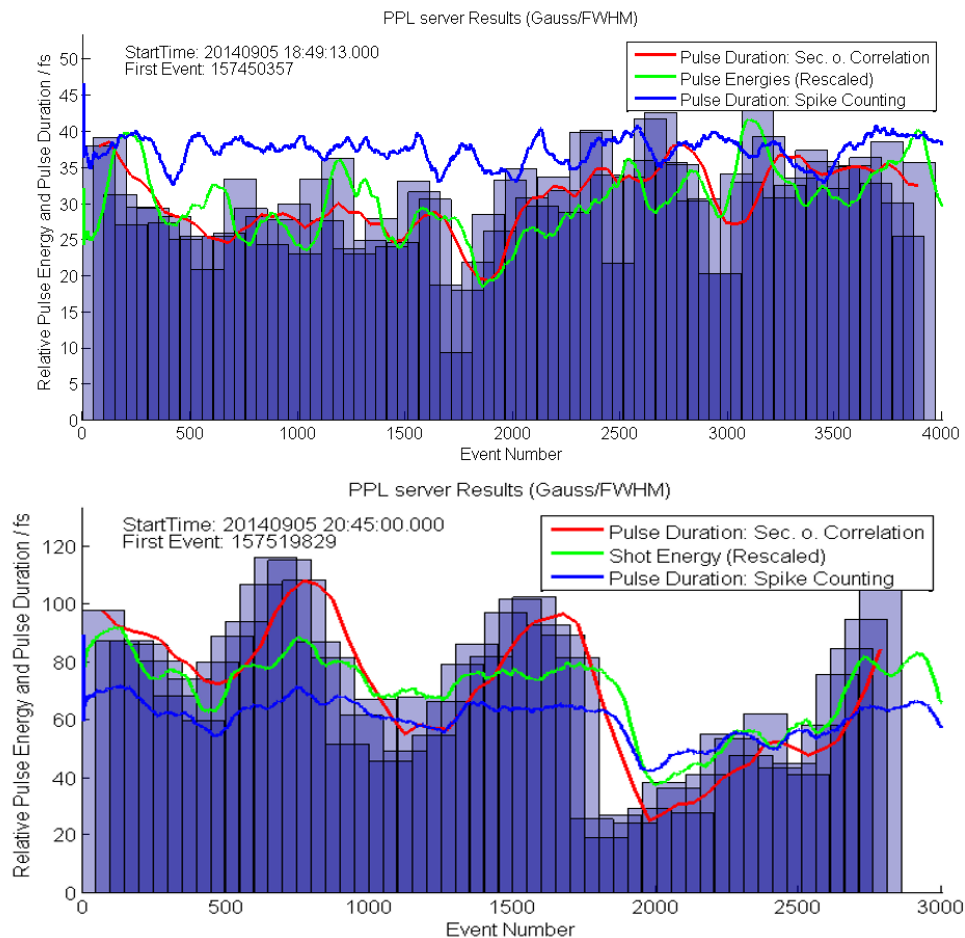


FIGURE 6.1: The graphs show the temporal development of the measured pulse duration in comparison to the relative shot energy. The blue bars each represent single measurements, the red line the averaged pulse duration measured with second order correlation method, the blue line is measured with the spike counting method. The green line shows the averaged shot energy, normalized to fit the scale. Measurement taken 05.09.2014, upper plot 20:45 to 20:50, total of 2995 spectra; lower plot 18:49 to 18:56, total of 4053 spectra, each second order correlation calculation considered a package of 150 spectra.

Figure 6.1 shows a comparison between the measured photon pulse duration and the shot energy. At several measurement shifts the results of the PPL server exhibited strong variations on a time scale of minutes. This could be an effect of unstable beam

conditions or of errors in the measurement method.

If the fluctuations represent the real beam parameters, similar fluctuations should be found in other characteristic parameters of the photon pulse. We chose the FEL shot energy² for comparison, because it is a reliably measurable parameter.

As expected, a general correlation of the fluctuations in photon pulse energy and measured photon pulse duration can be observed. Interestingly, the second order correlation method appears to respond stronger to the fluctuation of photon pulse energy. However, both photon pulse duration measurements result in similar average results and show a temporal correlation to the photon pulse energy. Considering these observations, it seems likely that the fluctuations of the measured photon pulse duration represent the real fluctuations of the photon pulse duration.

²These shot energies are calculated by integration of the spectral intensity over the full spectrum.

6.2 Apertures in the Photon Beam

A simple way to manipulate the FEL beam is to select a part of the transversal beam profile by the usage of apertures. At a first glance, if the beam is transversely coherent, the apertures should have no significant effect on the measurement. Possible higher transverse modes in the beam could lead to an influence of the apertures on the measurement result. To observe this, measurements with apertures of varied width and height were taken using the water-cooled aperture unit (WAU). The results are shown in Figure 6.2.

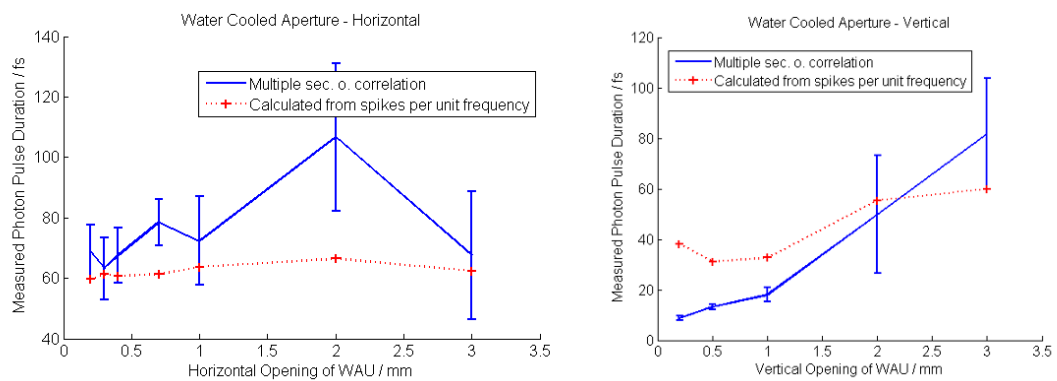


FIGURE 6.2: Measurement with different apertures. The vertical apertures correspond to the dispersive direction of the spectrometer. Measurements taken 05.09.2014 between 19:44 and 20:50.

It must be remarked that the FEL conditions during these measurements were very unstable³. The measurements fluctuate strongly and show large errors⁴. Nevertheless, some general trends can be observed:

- The measured pulse duration decreases at small apertures in the dispersive direction of the spectrometer.
- The second order correlation method is more affected than the spike-counting method.
- The error-bars decrease at small apertures, especially in vertical direction.

We observe that the horizontal apertures had a different effect as compared to the vertical apertures. This is likely caused by the spectrometer dispersion working along the vertical

³They are taken in the same time-frame as the measurements for temporal stability, c.f. Figure 6.1.

⁴The displayed error-bars represent the standard deviation of the multiple correlation results.

axis. Horizontal apertures slightly reduce the error-bars in the measurement. Due to the large fluctuation in the measured pulse durations, we can not deduce a systematic influence of the horizontal aperture on the average measurement result. However, the error-bars seem to be slightly reduced by the horizontal apertures. They could therefore be attractive as a measure of "pulse cleansing" in future measurements.

Vertical apertures have a significant effect on the measurement, reducing the apparent pulse duration for both spike counting and second order correlation method, although the latter is much stronger affected. One explanation is the additional diffraction at the aperture along the dispersive axis. The magnitude of such a diffraction is estimated in Appendix C. Such diffraction can explain the results for small vertical apertures, as the spike width is no longer determined by the FELs spectral coherence, but by the diffraction at the aperture. As the diffraction is only dependent on the aperture width and therefore constant over each measurement, the fluctuation in apparent pulse duration (i.e. error-bars) is drastically reduced. The spectra appear to the second order correlation method to have a larger spectral coherence and consequently a shorter pulse duration. The number of spectral spikes is affected only indirectly, as close widened spikes can no longer be distinguished. The altered results can not be used as valid measurements, as information about the photon pulse is lost in the additional diffraction.

6.3 Electron Bunch Charge

In this experiment we varied the charge of the lasing electron bunch. The intention is to get a good comparison of the non-dispersive electron bunch duration measurements taken with the LOLA TDS and the second order correlation and spike counting measurements of the photon pulse⁵. The results are shown in Figure 6.3. Because we want to compare three different physical parameters, the results from the LOLA measurements were rescaled to fit the scale⁶. The exact measured values are listed in Table 6.1.

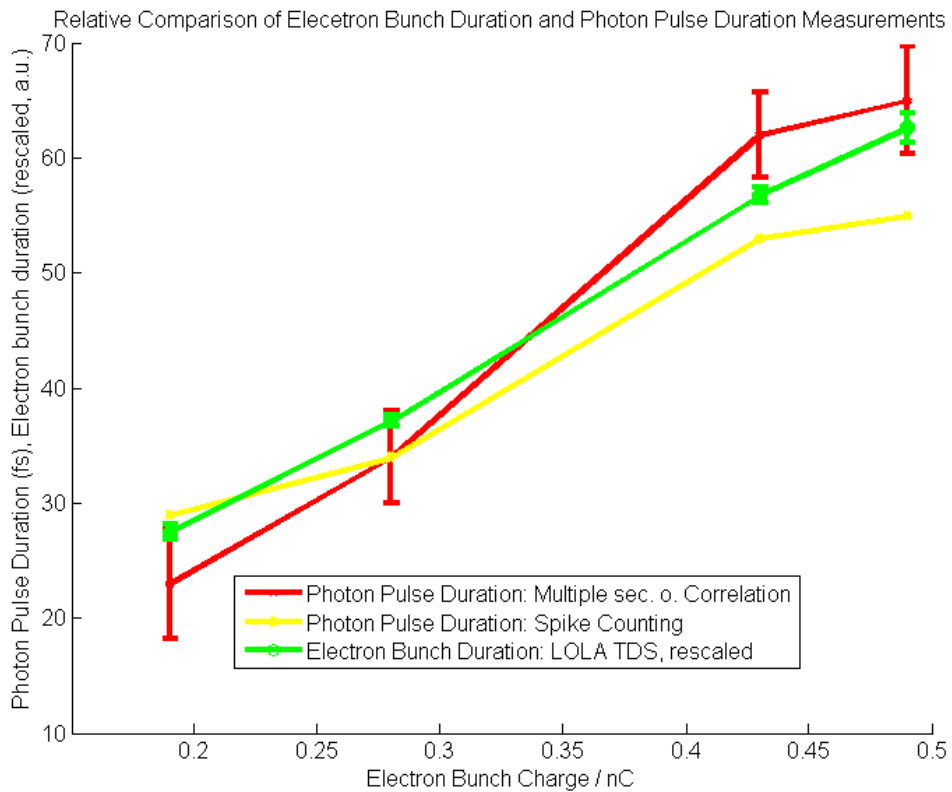


FIGURE 6.3: Second order correlation and spike counting measurements compared to measurements of the electron bunch duration with varied electron bunch charges. Measurements taken 05.09.2014 between 22:07 and 22:29.

It should be noted that the results of the second order correlation method contain an additional systematic error, as the SASE gain bandwidth might have changed during the returning process.

⁵This was done without retuning the accelerator phase, as this would change the shape of the electron bunch and thereby the profile function (See Equation 3.18).

⁶The values were rescaled so that their average matches the average result of the multiple second order correlation measurements.

Measurement with different bunch charges

Start	End	Charge / nC	LOLA / fs	Correlation / fs	Spike Counting / fs
22:07	22:14	0.49	278	65	55
22:14	22:18	0.43	252	62	53
22:19	22:23	0.28	165	34	34
22:24	22:29	0.19	122	23	29

TABLE 6.1: Comparison of electron bunch duration measurements using the LOLA TDS (rms) and the photon pulse duration measured by the multiple correlation method (single line spectra) and the spike counting method at different electron bunch charges. Taken 05.09.2014.

We observe a near-linear dependence between electron bunch charge, electron bunch duration and photon bunch duration, as long as the bunch shape is kept more or less constant. On this relative scale, the three measurements exhibit a standard deviation of about $\sigma = \pm 6.8\%$ to each other. This relative accuracy exceeds our expectations even though it bases on only four measurements.

Chapter 7

Conclusion and Outlook

The photon pulse duration is an important parameter in the FEL tuning process and in many FEL experiments. Despite its importance and a variety of proposed measurement techniques [10], the beamline diagnostic of FLASH does not provide any permanently available pulse duration measurement techniques.

I have successfully developed software for the evaluation of XUV SASE FEL photon pulse spectra, resulting in an estimation of the photon pulse duration. While other photon pulse duration measurements usually require additional experimental end-stations, all measurements required for my software can be performed with the standard beamline equipment installed at FLASH without any additional set-up. The implemented algorithms make use of second order spectral correlations, analysis of spectral intensity spiking and considerations of the pulse energy probability density distribution.

An application has been programmed in MATLAB, enabling a simple and quick usage of all three methods for pulse duration measurement. The second order correlation method has additionally been realized in an on-line measurement tool and permanently integrated to the data acquisition system at FLASH.

For the first time it provides machine operators with a real-time feedback about the photon pulse duration, which can be an important parameter during FEL tuning.

The SSA GUI further provides tools for detailed analysis of recorded spectra that might be of interest in future research, not only for the consideration of the photon pulse duration, but also of FEL regime, machine stability or other parameters.

The specification of absolute measurement accuracy remains unknown, since no other photon pulse length measurement technique was available for a direct comparison. However, the spike counting and second order correlation methods have been compared to the electron pulse duration measurements of the transverse deflecting structure LOLA, exhibiting a relative accuracy of $\sigma = \pm 6.8\%$. Furthermore, comparisons with the temporal fluctuations in the photon pulse energy indicate a good temporal resolution of the second order correlation and spike counting methods.

The current absolute measurement accuracy should be verified by further experiments, but the good relative accuracy and small experimental effort already make the presented tools well suited for tuning purposes and relative measurements.

Although the presented tools already achieve very good results, I still see a big potential for further optimization of the methods.

I therefore hope to see photon pulse duration analysis by second order spectral correlations becoming a standard procedure in future FEL operation.

Appendix A

MATLAB: Spectra Evaluation

This chapter contains a selection of the most essential MATLAB functions that are used for the spectra evaluation for photon pulse duration. A collection of all used scripts can be found in [18].

Gaussian Fit

This function calculates the theoretical second order correlation function for a Gaussian electron bunch shape.

```
1 function [sigmT, Result, fit_range, err] = GaussFit(g2, freqshift,
2         fit_range_limit, fit_range_offset, sigmT)
3 global DEBUG
4 %least-squares fitting:
5 beforeFit =toc;
6 err = 'ok\n';
7 fit_range = 1;
8
9 %% Check Input
10 if numel(g2) <= 1
11     Result = -1;
12     err = 'numel(g2)<=1\n';
13     return
14 end
15
16
```

```

17 %% Define function
18 % The factor 1e15 sets calculations to fs and makes calculations faster
19 G2_fun_g = @(sigmT, Xvector) 1+(exp(-Xvector.^2*2*(sigmT*1e-15).^2/2))*double
    (g2(1)-1); %simplified
20
21 %% Find correlation range
22 while g2(fit_range) >= g2(1)-(g2(1)-1)*fit_range_limit
23     fit_range = fit_range+1;
24     if fit_range==length(g2), break, end
25 end
26 fit_range = fit_range + fit_range_offset;
27 temp = 'ok';
28 if fit_range < 1
29     fit_range = 1;
30     temp = 'Fit range negative';
31 end
32 if fit_range > length(g2)
33     fit_range = length(g2);
34     temp = 'Fit range too large';
35 end
36
37 if ~(strcmp(temp, 'ok')),
38     err = temp;
39 end
40
41 %fit_range = length(g2); %Disable limited fit range
42
43 %% Fit for optimal time parameter
44 %[Messages, sigmT]=evalc('lsqcurvefit(G2_fun_g, sigmT, freqshift, double(g2))')
    ; % Theoretical Values
45 [sigmT, temp]=(lsq(freqshift(1:fit_range), double(g2(1:fit_range))), G2_fun_g,
    sigmT); % Theoretical Values %self-written function
46
47 if ~(strcmp(temp, 'ok\n')),
48     err = sprintf('%s, %s \n', err, temp);
49     if (DEBUG~=0), fprintf(temp), end
50 end
51
52 Result = G2_fun_g(sigmT, freqshift);
53
54 %%

```

```

55 switch DEBUG
56     case 8
57         fprintf('Fitting took %f ms \n',(toc-beforeFit)*1000)
58     case 6
59         fprintf(err);
60 end

```

The fitting function for rectangular electron bunch form works similarly, using a different function `G2_fun_g`.

Least Squares Optimization

This specialized gradient based least squares optimization algorithm is used instead of the MATLAB inherent eigenvalue based `lsqcurvefit` because of its faster run-time. It is called by all second order correlation calculations with automated fitting.

```

1 function [param, err] = lsq(X,Y,fun,param0)
2 %LSQ      Least Squares
3 % Finds the first minimum of the summed squared difference between
4 % the input X and fun(param,x) in terms of param .
5 % the inputs should be:
6 % X:      A vector of real x-Values
7 % Y:      A vector of real y-values to which param should be fitted , length
8           must be the same as X
9 % fun:    A function handle accepting an x value and a parameter (both
10          scalar)
11 % param0: A starting parameter at wich the function will start computing.
12 %         The function will only find the frist minimum next to this value
13 %By Robin Engel, June 2014
14 tic
15 err = 'ok\n';
16
17 if param0 <= 1e-5, param0 = 15; end %preventing too small param0
18
19 if fun(param0,X(2)) == 1 %preventing too large param0
20     param0 = 100;
21 end

```

```
21 start_param = param0;
22 accuracy = 1e-5;
23 step = 0.1*param0;
24 last_direct = 0;
25
26
27
28 while step > accuracy
29
30     param1 = param0 - step;
31     param2 = param0 + step;
32
33     %finding the squared difference
34
35     summe= sum( (2*( Y-fun(param1,X) ) ./ (Y+fun(param1,X)) ).^2 );
36
37     sq1=sqrt(summe);
38
39     summe= sum( (2*( Y-fun(param2,X) ) ./ (Y+fun(param2,X)) ).^2 );
40
41     sq2=sqrt(summe);
42
43     %proceeding in the direction of the minimum
44     Diff = sq2-sq1;
45     if (Diff > 0)
46         param0 = param1;
47         direction = -1;
48     elseif (Diff < 0)
49         param0 = param2;
50         direction = +1;
51     else
52         param = param0;
53         err = 'Fit Fatal: Gradient too small for machine accuracy\n';
54         break
55     end
56
57     %reducing step size if a minimum was crossed
58
59     if ~(direction==last_direct)&&~(last_direct==0), step = step*0.5; end;
60     last_direct = direction;
```

```

61     if (toc>0.8), err = 'Fatal: Fitting time exceeded 0.8 seconds, breaking
        call\n';
62         break,
63     end
64 %     close    This can monitor the fitting cycle
65 %     figure(3)
66 %     hold on
67 %     plot(X, fun(param0,X))
68 %     plot(X,Y,'r')
69 %     hold off
70 %     keyboard
71 end
72 if (param0 == start_param), err = sprintf(err, 'Parameter not changed during
        Least-Squares Process\n');, end
73 param = param0;

```

Count Maxima

This function is used to count the spectral spikes in all spectra contained in the matrix `I_LP`¹.

```

1 function [Peak_Count, Peak_Count.FWHM, I_LP_Cut] = Count_Maxima(I_LP, wav,
        Isum, FWHMdat, Imin)
2 disp(' ... Spikes are being calculated ... ');
3
4 Peak_Count=zeros(1, size(I_LP,2)); %Anzahl Maxima aller Linien
5 Peak_Count_FWHM=zeros(1, size(I_LP,2)); %Anzahl der Maxima innerhalb der
        FWHM aller Linien
6
7
8 I_LP_Cut = I_LP;
9
10 for l=1:size(I_LP,2); %Geht spaltenweise (spektrenweise) durch
11     for k= 1:size(I_LP,1)%Lower level cut-off
12         if I_LP_Cut(k,l) < Imin*max(Isum)
13             I_LP_Cut(k,l)= NaN;
14         end
15     end

```

¹This matrix contains all currently loaded spectra, already subjected to the low-pass filter.

```
16
17
18   [~,imax2,~,~] = extrema(I_LP_Cut(:,1));           %counting single
   shot extrema %Returns indices of global maxima /R
19   % [~,imax2w,~,~] = extrema(I_LP(:,1)(FWHMdat.n1:FWHMdat.nr)); %
   counting single shot extrema within FWHMdat.n1:FWHMdat.nr window
20   imax2w=imax2(wav(imax2)<wav(FWHMdat.nr) & wav(imax2)>wav(FWHMdat.n1));
   %writes maxima index into imax2w, if it is in the FWHM window /R
21   Peak_Count_FWHM(1)= length(imax2w);
22   Peak_Count(1)= length(imax2);
23 end
24
25 disp(['Average No of spikes is Peak_Count= ',num2str(mean(Peak_Count))]);
26 disp(['Average No of spikes within FWHM is Peak_Count_FWHM= ',num2str(mean(
   Peak_Count_FWHM))]);
27
28
29 end
```

Appendix B

MATLAB: Data Handling

This chapter shows a selection of essential auxiliary scripts.

SaveDAQdata

This script is used to read recorded data from the DAQ storage.

```
1 % Skript to read data fromn DAQ and save then as mat files
2 %Author: Robin Engel
3
4 XMLfilename = input('Please enter the name of the XML file\n', 's');
5
6 [data, timing] = my_read_daq_data(XMLfilename) ;
7
8 save(sprintf('DataFrom%s', XMLfilename(1:end-4)));
```

my_read_daq_data

This is a function called by `SaveDAQdata`.

```
1 function [data, times] = my_read_daq_data(XMLfilename)
2
3 %MY_READ_DAQ_DATA Reads float values from the daq and retruns them as a
4 %matrix
5 % The Returned vector 'data' is a 1xX matrix, where X is the amount of
```

```
6 % data points found from the daq files .
7 % The matrix 'times' contains the the
8 % timing information of the corresponding values .
9 %Author: Robin Engel
10 [Outputs,a,err] = evalc('daq_read_svr(XMLfilename)');
11
12 afields = fieldnames(a);
13
14 for i=1:numel(afields)
15     temp1 = getfield(a,afields{i});
16     if(~exist('location','var'))
17         temp3 = fieldnames(temp1);
18         location = temp3(1);
19     end
20     temp2 = getfield(temp1,char(location));
21     data(1,i) = temp2;
22     times(1,i) = temp1.time(1);
23     times(2,i) = temp1.time(2);
24     times(3,i) = temp1.time(3);
25 end
```

Averaging Signals

This script was used to smooth signals with large noise.

```
1 function avg_vec = average_over_N(vec,N)
2
3 %Average vector over the last N points
4 % avg_vec = average_over_N(vec,N)
5 % This functions reads in a vecot and returns a smoothed vector ,
6 % in which the vvalues are averaged over the last N points.
7 % The default value for N is 100
8 % The dimension of the vector does not matter, but the other must be one.
9 % (No matrices accepted)
10
11 if ~exist('N')
12     N = 100;
13 end
14
```

```
15 avg_vec = zeros(size(vec,1),size(vec,2));
16
17 for i = 1:length(vec)
18     if i>N
19         n = N-1;
20     else
21         n = i-1;
22     end
23
24     avg_vec(i) = mean(vec(i-n:i));
25 end
```

Appendix C

Diffraction from WAU

When the WAU are closed in only one direction, their effect can be described as a single slit diffraction experiment. The first minimum of diffraction can be expected at an angle α of

$$\sin \alpha = \frac{\lambda}{d} \sim \alpha \quad (\text{C.1})$$

, where d is slit width and λ is the radiation wavelength. The distance L from the WAU to the spectrometer screen is about 20 meters. The distance x between diffraction maximum and first minimum is therefore

$$x = L * \tan(\alpha) \sim \alpha L. \quad (\text{C.2})$$

Combining Equations C.1 and C.2 we obtain

$$x \sim \frac{\lambda}{d} L \quad (\text{C.3})$$

At FLASH, the wavelength is in the order of 10nm and the WAU have a width of about 1mm. We conclude for the dimension of x :

$$x \sim \frac{10^{-8}m}{10^{-3}m} 20m \sim 200\mu m \quad (\text{C.4})$$

Compared to the pixel size of the ICCD camera of the spectrometer, which is in the order of $10\mu m$, the diffraction from WAU slits can be significant.

Bibliography

- [1] S. Schreiber, B. Faatz, J. Feldhaus, K. Honkavaara, and R. Treusch. Fel user facility flash. In *Proc. of the 2010 International Particle Accelerator Conference*, 2010.
- [2] Svitozar Serkez. Analysis of statistical properties of flash radiation in spectral domain to characterize pulse duration. Master thesis, Ivan Franko Lviv National University and Deutsches Elektronen Synchrotron, 2012.
- [3] W. Ackermann, G. Asova, V. Ayvazyan, A. Azima, N. Baboi, J. Bähr, V. Balandin, B. Beutner, A. Brandt, A. Bolzmann, et al. Operation of a free-electron laser from the extreme ultraviolet to the water window. *Nature photonics*, 1(6):336–342, 2007.
- [4] Samuel Krinsky and RL Gluckstern. Analysis of statistical correlations and intensity spiking in the self-amplified spontaneous-emission free-electron laser. *Physical Review Special Topics-Accelerators and Beams*, 6(5):050701, 2003.
- [5] Evgenij L. Saldin, Evgeny A. Schneidmiller, and Mikhail V. Yurkov. Statistical properties of the radiation from vuv fel at desy operating at 30nm wavelength in the femtosecond regime. *Nuclear Instruments and Methods in Physics Research Section A: Accelerators, Spectrometers, Detectors and Associated Equipment*, 562(1):472–486, 2006.
- [6] M. Martins, M. Wellhöfer, J.T. Hoeft, W. Wurth, J. Feldhaus, and R. Follath. Monochromator beamline for flash. *Review of scientific instruments*, 77(11):115108, 2006.
- [7] L Fröhlich, O Grimm, K Klose, M Nagl, O Peters, J Rossbach, H Schlarb, Germany M Ross, TJ Smith, D McCormick, et al. Longitudinal bunch shape diagnostics with coherent radiation and a transverse deflecting cavity at ttf2. 2004.

- [8] Minjie Yan. Suppression of cotr in electron beam imaging diagnosis at flash. Technical report, Deutsches Elektronen-Synchrotron (DESY), Hamburg (Germany), 2011.
- [9] M. Wellhoefer. *The Monochromator Beamline at the Free Electron Laser in Hamburg: (FLASH) ; Assembly, Characterization, and First Experiments*. Verlag Dr. Hut, 2007. ISBN 9783899635850.
- [10] S. Duesterer. Development of experimental techniques for the characterization of ultrashort photon pulses of xuv free-electron lasers. *Physical Review Special Topics-Accelerators and Beams*, 15:030705, 2012.
- [11] Evgenij L. Saldin, Evgeny A. Schneidmiller, and M. V. Yurkov. Statistical properties of radiation from vuv and x-ray free electron laser. *Optics Communications*, 148(4):383–403, 1998.
- [12] AA Lutman, Y Ding, Y Feng, Z Huang, M Messerschmidt, J Wu, and J Krzywinski. Femtosecond x-ray free electron laser pulse duration measurement from spectral correlation function. *Physical Review Special Topics-Accelerators and Beams*, 15(3):030705, 2012.
- [13] S.V. Milton, E. Gluskin, N.D. Arnold, C. Benson, W. Berg, S.G. Biedron, M. Borland, Y.-C. Chae, R.J. Dejus, P.K. Den Hartog, et al. Exponential gain and saturation of a self-amplified spontaneous emission free-electron laser. *Science*, 292(5524):2037–2041, 2001.
- [14] E. L. Saldin, E. A. Schneidmiller, and M.V. Yurkov. *The Physics of Free Electron Lasers*. Springer, 1999. ISBN 9783540662662.
- [15] C. Behrens, N. Gerasimova, Ch. Gerth, B. Schmidt, E. A. Schneidmiller, S. Serkez, S. Wesch, and M. V. Yurkov. Constraints on photon pulse duration from longitudinal electron beam diagnostics at a soft x-ray free-electron laser. *Phys. Rev. ST Accel. Beams*, 15:030707, Mar 2012. doi: 10.1103/PhysRevSTAB.15.030707. URL <http://link.aps.org/doi/10.1103/PhysRevSTAB.15.030707>.
- [16] S. Krinsky and Z. Huang. Frequency chirped self-amplified spontaneous-emission free-electron lasers. *Phys. Rev. ST Accel. Beams*, 6:050702, May 2003.

- [17] Michael Röhrs. *Investigation of the Phase Space Distribution of Electron Bunches at the FLASH-Linac Using a Transverse Deflecting Structure*. PhD thesis, Universität Hamburg, Fachbereich Physik, 2008.
- [18] Robin Engel. Complete collection of matlab-scripts used for "real time analysis of fel radiation spectra for the estimation of photon pulse duration", jan 2015. URL <http://www.desy.de/~engelr/>.
- [19] Engel, Robin. Implementation of the Photon Pulse Length Middle Layer Server into the Data Acquisition System at FLASH. Technical report, Deutsches Elektronen Synchrotron, Carl-von-Ossietzky Universität Oldenburg, Hochschule Emden-Leer, 2014.
- [20] Doocs java applications at desy, December 2014. URL <http://tesla.desy.de/common/applications/index.jsp>.

Contributions

The second order correlation method for photon pulse length estimation was presented in form of a Poster at the *Science@FELs* Conference 2014 at the Paul Scherrer Institute under the title *Real time analysis of FEL radiation spectra for the determination of the photon pulse duration* and was awarded as the best new development Poster.

Declaration of Authorship

I hereby certify that this thesis has been composed by me and is based on my own work except where indicated otherwise. I have not used any references or verbatim extracts other than those quoted, and all sources of information, including graphs and data sets, have been specifically acknowledged. Additionally I certify that I followed the general principles of scientific work and publication, as they are specified in the guidelines for good scientific practice of Carl-von-Ossietzky Universität Oldenburg.

Date:

Signed: